



# Self-Consistent State-to-State Kinetic Modeling of CO<sub>2</sub> Cold Plasmas: Insights on the Role of Electronically Excited States

L. D. Pietanza<sup>1</sup> · G. Colonna<sup>1</sup> · M. Capitelli<sup>1</sup>

Received: 29 June 2023 / Accepted: 1 October 2023  
© The Author(s) 2023

## Abstract

This study focuses on the role of CO<sub>2</sub> and CO electronically excited states in the kinetics of CO<sub>2</sub> cold non-equilibrium plasma discharges by means of a state-to-state OD kinetic model based on the simultaneous and self-consistent solution of the electron Boltzmann equation and the master equations describing the vibrationally and electronically excited state kinetics and the plasma composition. A new CO<sub>2</sub> dissociation model based on the use of the Biagi electron impact excitation cross sections, considered as fully dissociative, of several CO<sub>2</sub> electronic excited states, in the energy range from 6.5 to 25 eV, is tested and compared with the results obtained by using the Phelps database in typical glow and microwave discharge conditions. Moreover, a refinement of the kinetics of the CO(*a*<sup>3</sup>Π) excited state is proposed by including new production and loss terms and the effect of the change of its time evolution density on the eedf, the electron temperature, the CO<sub>2</sub> and CO vibrational distribution functions, electron impact and vibrational induced dissociation rates is investigated. Finally, the contribution of the CO(*a*<sup>3</sup>Π) state to CO<sub>2</sub> dissociation is examined in terms of production and recombination (or back-reaction) processes both in microwave and glow discharge conditions.

**Keywords** CO<sub>2</sub> · Electronically excited states · State-to-state models · Self-consistent models · Electron Boltzmann equation · Vibrational kinetics

## Introduction

In the last decades, the increased emission of greenhouse gas (mainly carbon dioxide) and the decreasing reserves of traditional energy sources have renewed the interest in CO<sub>2</sub> conversion by cold non-equilibrium plasmas as a valid alternative to conventional route to increase the energy efficiency of CO<sub>2</sub> conversion. Plasma discharges provide a favorable environment for activating the CO<sub>2</sub> gas by electron impact excitation (vibrational and electronic), increasing CO<sub>2</sub> reactive channels at relatively low gas temperature. Among the complex reactions involved in the conversion chain, the CO<sub>2</sub> dissociation is a key process

---

✉ L. D. Pietanza  
luciadaniela.pietanza@cnr.it

<sup>1</sup> CNR-ISTP, Consiglio Nazionale delle Ricerche, Istituto per la Scienza e Tecnologia dei Plasmi, via Amendola 122/D, 70126 Bari, Italy

affecting the overall efficiency. Besides the direct electron impact mechanism, CO<sub>2</sub> dissociation can also occur by selectively pumping energy into the lowest vibrational levels through electron-vibrational (eV) collisions, followed by vibrational-vibrational (VV) processes, which populate the upper vibrational levels inducing dissociation from these levels. This vibrational induced dissociation process has a maximum threshold energy of 5.5 eV, lower than the threshold values of the dissociation cross sections by electron impact, increasing the energy efficiency of CO<sub>2</sub> dissociation. For this reason, a strong interest in the scientific community has been channeled towards the investigation of the conditions in which vibrational excitation can be maximized in non-equilibrium plasma discharges for a more energy efficient CO<sub>2</sub> dissociation [1].

Different discharge configurations have been numerically and experimentally investigated for CO<sub>2</sub> conversion characterized by different values of pressure, gas temperature, applied power density and/or electric field and residence time in the discharge, i.e. direct current (DC) glow or radio frequency (RF) discharges [2, 3], moderate- and high-pressure microwave (MW) discharges [4–6], atmospheric-pressure dielectric barrier discharges (DBD) [7–9], nanosecond repetitively pulsed discharges (NRPD) [10, 11], gliding arc (GA) discharges [12].

CO<sub>2</sub> plasmas are also important for aerospace applications, such as the study of spacecraft entry in Mars and Venus atmosphere [13] or oxygen production on Mars for in-situ resource utilization in future space exploration missions [14]. The use of nonequilibrium plasma for CO<sub>2</sub> dissociation is also important for biomedical applications. As an example, a helium plasma jet with a 1% CO<sub>2</sub> admixture was used to produce small amounts of CO in safe conditions for the treatment of various human health diseases thanks to its anti-inflammatory, vasodilator, anti-apoptotic and anti-proliferative effects [15].

The understanding of the chemistry of non-equilibrium CO<sub>2</sub> reactive plasmas is a challenging problem and needs the implementation of advanced plasma kinetic modeling. The most refined kinetic simulation description is provided by the State-To-State (STS) approach [16, 17] in which the population density of each excited state of atoms and molecules is followed by taking into account the relevant involved reaction processes. This approach becomes essential when the chemistry is dependent on the high lying vibrational or electronic excited states. The corresponding time dependent balance equations involve the rate coefficients of each considered reaction. The rate coefficients of heavy particle collisions are in general gas-temperature dependent and are often described by using Arrhenius rates taken from the literature. The rate coefficients of electron impact processes are calculated from the energy-dependent cross sections and the electron energy distribution function (eedf), which can be obtained by solving the electron Boltzmann equation. The electrons have a key role in CO<sub>2</sub> dissociation in non-equilibrium plasma discharges. They can directly dissociate CO<sub>2</sub> molecules and transfer part of the discharge energy to atoms and molecules by means of inelastic collisions, exciting vibrationally and electronically states, and initiate the climbing of the vibrational ladder up to molecular dissociation. Excited states, in turn, give energy back to the electrons by superelastic collisions, affecting the eedf shape, by creating characteristic peaks [18], and, as a consequence, the calculation of the corresponding electron impact rates. The described scenario confirms the strong coupling between the electron and heavy particle kinetics, showing the importance of using an approach in which the STS master equations describing the vibrational and electronic excited state kinetics of heavy particles are solved simultaneously and self-consistently with the electron Boltzmann equation [1].

In this contribution, we present the results obtained by using an advanced 0D self-consistent STS kinetic model for the description of CO<sub>2</sub> reactive plasma mixture in

non-equilibrium plasma discharge and post-discharge conditions [19]. The model provides a complete characterization of the plasma mixture calculating the temporal evolution of chemical species densities, the vibrational distribution functions (vdf) of the molecules, the electronic excited state densities and the eedf in discharge and post-discharge conditions characterized by different conditions of pressure and gas temperature, applied power density and/or electric field and residence time in the discharge. A brief description of the model will be presented in section “[Brief description of the kinetic model](#)”.

A special attention will be addressed to the investigation of the role of CO<sub>2</sub> and CO electronic excited states in the kinetics. For the CO<sub>2</sub> system, the Phelps database provides two electronic excited state excitation cross sections corresponding to threshold 7 and 10.5 eV. However, other CO<sub>2</sub> electronic excited states up to 12 eV have been identified by means of absorption spectroscopy and electronic structure calculations [20, 21] with corresponding electron impact excitation cross sections and a brief literature review of these states and a discussion about the possible inclusion in the kinetics is provided in section “[CO<sub>2</sub> electronic excited states: a literature review](#)”. The availability in the LXCat [22] of a new database of electronic excitation cross sections for CO<sub>2</sub>, i.e. the Biagi dataset [23, 24], has pushed towards the testing of a new dissociation model via electronic excitation in which these cross sections are considered fully dissociative, and the comparison with the dissociation model linked to the Phelps database (see section “[CO<sub>2</sub> electron impact dissociation model via electronic excitation](#)”). A focus on the first electronic excited state of CO molecules, i.e. CO(a<sup>3</sup>Π) at 6 eV is performed in section “[A focus on kinetics](#)”, with a refinement of its kinetics by including new production and loss processes. This electronic state affects the vibrational kinetics of CO ground state molecules by means of the quenching process CO(a<sup>3</sup>Π) + CO → CO(v = 27) + CO [25] with a pumping of vibrational quanta in the CO vdf, giving also a contribution to CO<sub>2</sub> dissociation/recombination (see section “[Contribution of the to CO<sub>2</sub> dissociation](#)”). Conclusions and perspectives are presented in section “[Conclusions and perspectives](#)”. Finally, the Appendix reports some tables related to the energy levels and the reaction processes included in the model.

## Brief Description of the Kinetic Model

The plasma kinetics is described by a 0D self-consistent time dependent model in which the electron Boltzmann equation is solved simultaneously and self-consistently with the non-equilibrium state-to-state master equations describing the vibrational, the electronic excited state kinetics and the plasma chemistry of the reacting mixture. The corresponding general equations are the followings:

- (1) the electron Boltzmann equation, in the homogeneous and quasi-isotropic approximations (two term expansion) developed by Rockwood [26], see also [27–29]

$$\frac{\partial n(\varepsilon, t)}{\partial t} = -\frac{\partial}{\partial \varepsilon} (J_E + J_{el} + J_{ee}) + S_{in} + S_{sup} + S_{rct,f} + S_{rct,b} \quad (1)$$

where  $n(\varepsilon, t)$  represent the number density of electrons with energy between  $\varepsilon$  and  $\varepsilon + d\varepsilon$ , linked to the  $f(\varepsilon, t)$ , i.e. the eedf in eV<sup>-3/2</sup>, by  $f(\varepsilon, t) = \frac{n(\varepsilon, t)}{n_e(t)} \varepsilon^{-3/2}$ , where  $n_e(t)$  is the total electron number density. The first three terms on the right hand side of Eq. (1) correspond to fluxes of the electrons along the energy axis due to electric field ( $J_E$ ), elastic electron-molecule ( $J_{el}$ ) and electron–electron ( $J_{ee}$ ), while the last two

sources terms are due to inelastic ( $S_{in}$ ) and superelastic ( $S_{sup}$ ) (vibrational and electronic) collisions and electron-induced chemical reactions, such as dissociation and ionization processes ( $S_{rct,f}$ ) and their reverse ones ( $S_{rct,b}$ ).

- (2) the state-to-state vibrational kinetic equations accounting for the relevant energy exchange and reactive processes induced by collisions with electron and heavy-particles

$$\begin{aligned} \frac{dN_v}{dt} = & \left( \frac{dN_v}{dt} \right)_{eV} + \left( \frac{dN_v}{dt} \right)_{VT} + \left( \frac{dN_v}{dt} \right)_{VV} + \left( \frac{dN_v}{dt} \right)_{VV'} \\ & + \left( \frac{dN_v}{dt} \right)_{VE} + \left( \frac{dN_v}{dt} \right)_{SE} + \left( \frac{dN_v}{dt} \right)_{React} \end{aligned} \quad (2)$$

where  $N_v$  is the vibrational distribution in the  $v$ th vibrational level and, on the right-hand side, the terms due to the contribution of electron-vibration (eV), vibration-to-translational (VT), intramode (VV) and intermode (VV') vibration–vibration, vibrational-to-electronic (VE), spontaneous emission (SE) processes and to the relevant reactive channels, such as, for example, dissociation and ionization processes and their reverse.

- (3) the state-to-state electronic excited state kinetic equations of atoms and molecules

$$\frac{dN_i}{dt} = \left( \frac{dN_i}{dt} \right)_{eE} + \left( \frac{dN_i}{dt} \right)_{SE} + \left( \frac{dN_i}{dt} \right)_{Quench} \quad (3)$$

where  $N_i$  is the number density of the  $i$ th electronic excited state and the terms on the right-hand side correspond to excitation/de-excitation by electron impact (eE), spontaneous emission (SE) and quenching by heavy-particle (Quench) collisions.

- (4) the equation describing the plasma chemistry of the different species (neutral and ionized)

$$\frac{dn_s}{dt} = \sum_j \left\{ \left( K_j \left[ a_{sj}^R - a_{sj}^L \right] \right) \right\} \quad (4)$$

where  $n_s$  is the density of the  $s$ th specie,  $j$  the reaction index,  $a_{sj}^R$  and  $a_{sj}^L$  are the right- and left-hand side stoichiometric coefficients of the species  $s$  taking part of the reaction  $j$ ,  $K_j$  is the reaction rate calculated as  $K_j = k_j \prod_l n_l$ , where  $k_j$  is the rate coefficient and  $\prod_l n_l$  is the product of the densities  $n_l$  of the species present on the left side of reaction  $j$ .

The time-dependent self-consistent approach is based on the simultaneous solution of Eq. (1–4), which are strongly coupled. At each time step, the electron impact rate coefficients entering in Eq. (2–4) are calculated by integrating the eedf and the corresponding electron impact cross sections on the electron energy axis, while, the collisional terms entering in the electron Boltzmann equation (Eq. (1)) are calculated by using the vibrational distribution functions, the electronic excited state populations and the plasma composition calculated by Eq. (2–4).

The input parameters used in the model are the gas temperature  $T_{\text{gas}}$ , the pressure  $P$ , the reduced electric field  $E/N$  or the power density ( $P_d$ ) and the residence time ( $t_d$ ) in the discharge. These values ( $T_{\text{gas}}$ ,  $P$ ,  $E/N$ ,  $P_d$ ) can be assumed constant or with a fixed time dependent profile, following, for example, the experimental one, when available. In the post-discharge, i.e. for  $t > t_d$ , the reduced electric field and the power density are assumed equal to

zero. The electron density ( $N_e$ ) time profile is not fixed but self-consistently calculated from the solution of the chemical reactions involving the electrons, the ions and the heavy particles. If we use, as input parameter, the power density, the electric field is calculated from the  $P_d$  and  $N_e$  values according to the following relation  $P_d = J * E = v_d N_e q_e E = \mu_e N_e q_e E^2$ , where  $J$  is the discharge current density,  $v_d$  the drift velocity,  $\mu_e$  the electron mobility and  $q_e$  the electron charge. In particular, during the time evolution, at each time step  $t$ , starting from the values of  $P_d$ ,  $N_e$  and  $\mu_e$ , the electric field value  $E(t)$  is calculated from the above relation. Then, by solving the electron Boltzmann equation, the new eedf is calculated at  $t+dt$ , as well as the new electron mobility and new electron impact rates, which enter in the kinetic balancing equation, whose solution gives the new composition at  $t+dt$ , including the new electron density. This cycle is repeated at each time step.

The plasma mixture considered is characterized by the following species, i.e.  $\text{CO}_2$ ,  $\text{CO}$ ,  $\text{O}_2$ ,  $\text{C}$ ,  $\text{O}$ ,  $\text{CO}_2^+$ ,  $\text{CO}^+$ ,  $\text{O}_2^+$ ,  $\text{C}^+$ ,  $\text{O}^+$ ,  $e^-$ . For the  $\text{CO}_2$  system, the pure asymmetric mode levels of the kind  $(0, 0, v)$  up to the dissociation limit of 5.5 eV (21 levels) and few low lying symmetric and bending levels, i.e.  $(010)$  and the first three Fermi levels (see Table 6, Appendix), are accounted for, following the approach of Kozak et al. [30, 31]. The inclusion of higher lying symmetric, bending and Fermi levels and of all the mixing vibrational  $(v_1, v_2, v_3)$  levels, beneficial for increasing the reliability of the model, is still a difficult task due to the lack of complete sets of vibrational-state resolved electron impact cross section data and heavy particle vibrational energy exchange rate coefficients for the  $\text{CO}_2$  molecule, as discussed in [1].

Also the corresponding VV, VV' and VT rate coefficients have been derived following the approach of Kozak et al. [30, 31], i.e. by applying Schwartz-Slawsky-Herzfeld (SSH) scaling laws [32], starting from available theoretical and/or experimental rate coefficients involving low lying vibrational levels. Only mono-quantum transitions are accounted for. One electronic excited state of  $\text{CO}_2$  at 10.5 eV is also included as a metastable state.

A detailed vibrational and electronic excited state kinetics is also considered for the main  $\text{CO}_2$  dissociation products, i.e. the  $\text{CO}$  and  $\text{O}_2$  systems, taking into account, respectively, 80 and 34 vibrational levels and several electronic excited states with their related quenching and radiative processes [33–35]. The electron impact cross sections entering in the electron Boltzmann equation are taken from available database such as LXCat [22] and PHYS4ENTRY [36], which, unfortunately, do not provide all the needed vibrational-state resolved cross sections.

Scaling laws are used to account for missing electron impact cross sections. In particular, the Fridman's scaling law [37] has been applied to eV processes involving the  $\text{CO}_2$  asymmetric vibrational levels, i.e.  $e + \text{CO}_2(00v) \rightarrow e + \text{CO}_2(00w)$ , while a simple threshold shifting with the vibrational energy has been used for accounting for  $\text{CO}_2$  and  $\text{CO}$  ionization and dissociation cross sections.

Unfortunately, these scaling laws are based on semi-empirical formulas and more exact calculations based on quantum mechanical ab-initio methods are needed to better describe the vibrational-state dependence of the electron impact cross sections. In this direction, a significant effort has been made with the calculation of detailed electron impact vibrationally-resolved cross sections for the resonant channels in  $\text{CO}$  [38, 39] and  $\text{O}_2$  [40, 41], included in the model. A similar attempt has been also provided for the  $\text{CO}_2$  system [42] in the assumption of separation of the three modes and for vibrational levels up to  $v=10$  (transitions  $v_i \rightarrow v_j$  with  $0 \leq v_i \leq v_j \leq 10$  on each mode, keeping the other two quantum number at 0) but the missing of single-quantum transitions, due to the selection rule  $\Delta v = v_j - v_i = 2$  for the bending and asymmetric stretching modes, and of the non-resonant contribution, prevents, at the moment, the use of these data in the model.

CO<sub>2</sub> dissociation occurs via two different mechanisms:

- (1) direct electron impact (DEM)



- (2) pure vibrational (PVM and PVM<sub>O</sub>, respectively)



The electron impact dissociation from ground state (000) is described by the 7 eV Phelps cross section. The PVM and PVM<sub>O</sub> rate coefficients from ground were taken from literature [30, 31], while for higher vibrational levels, the Fridman-Macheret  $\alpha$  model is used [37].

According to this model, the vibrational energy ( $E_v$ ) lowers the activation energy ( $E_a$ ) of the process and the corresponding rate coefficient  $K_{PVM}(v)$  is calculated by multiplying the Arrhenius rate coefficient from ground  $K_0$  by a term dependent on a phenomenological  $\alpha$  coefficient ( $0 \leq \alpha \leq 1$ ), measuring the efficiency of lowering the reaction barrier by vibrational excitation, i.e.

$$K_{PVM}(v) = K_0 \exp\left(-\frac{E_a - \alpha E_v}{T_{gas}}\right) \quad (8)$$

$$(\text{if } E_v > E_a/\alpha, K_{PVM}(v) = K_0)$$

The list of the levels and reaction processes included into the model can be found in the Appendix and more detailed information on the kinetic model in [19].

Some model validation with results already present in literature were performed. In particular, the O<sub>2</sub>-O kinetics was validated by comparison with the modelling and the experimental results of Annusova et al. [43] in low pressure O<sub>2</sub> plasma discharges (P=10 mtorr–80 mtorr, T<sub>gas</sub>=620 K–900 K) finding a good agreement for the O<sub>2</sub> vdf, confirming the presence of a declining plateau in the range  $3 < v < 20$ , generated by the three body O atom recombination, i.e.  $\text{O} + \text{O} + \text{O} \rightarrow \text{O}_2(v) + \text{O}$  [44].

The model was also able to analyse the plasma conditions experimentally investigated by Groen et al. [6] for the CO<sub>2</sub> activation in MW discharges at high translational gas temperature ( $3500 \text{ K} < T_{gas} < 5500 \text{ K}$ ) [45]. By comparing the kinetic results with the corresponding thermodynamic ones, it was showed that the major components of the mixture, i.e. CO and O, could be described by the thermodynamic approach, while the other minor components presented large deviations from equilibrium. A qualitative agreement was found between experimental and theoretical values for the electron density, the E/N values and the electron temperature in both diffuse and contracted plasmas.

Recently, the model was applied to the description of glow discharge conditions at low pressure (P=5 torr), discharge current I=50 mA and residence time  $t_d=5$  ms [46] and its results compared to the modelling by Grofulovic et al. [47] and Silva et al. [48] and experimental results by Klarenaar et al. [3]. A good agreement was found for the low-lying CO<sub>2</sub> vibrational population densities and vibrational temperatures time evolution with comparable electron densities, stationary eedf and stationary reduced electric field values. The agreement is present as long as the electron density values predicted by our model are

comparable to Grofulovich's ones, showing the key role of eV processes for assessment of the vibrational excitation in glow discharge conditions.

The model has been used also to investigate the conditions for the activation of vibrational-induced dissociation of CO<sub>2</sub> in cold non-equilibrium plasma discharges [49]. These conditions are linked to the achievement of a sufficiently high non-equilibrium plateau in the CO<sub>2</sub> vdf due to the combining effect of eV and VV collisions, overpopulating higher vibrational levels and promoting dissociation. A satisfactory agreement of our simulation results with the Kotov's criterion [50] for vibrational-induced dissociation is found, confirming that the conditions for the onset of vibrational activation of the CO<sub>2</sub> dissociation process occurs for  $\left(\frac{Q}{N_0^2}\right) > \left(\frac{Q}{N_0^2}\right)^*$ , where Q is the power density and N<sub>0</sub> the initial CO<sub>2</sub> number density and  $\left(\frac{Q}{N_0^2}\right)^*$  is a threshold value which depends on the gas temperature and can be calculated from a semi-empirical balance equation for the vibrational energy by means of numerical simulations [50].

## CO<sub>2</sub> Electronic Excited States: A Literature Review

Electronic excited states of CO<sub>2</sub> have been studied both experimentally and theoretically. Several electron impact experiments with incident energy from threshold up to 100 eV [51, 52] and optical absorption experiments have been devoted to study low-lying electronic states of CO<sub>2</sub> [53, 54]. Moreover, many ab-initio calculations of CO<sub>2</sub> electronic structure, several assuming a linear geometry only, have been performed by using different methods with various levels of approximation [55–63]. At the moment, as also stated by Itikawa [20], there is no definite consensus about the assignment of the excited electronic-state energies of CO<sub>2</sub>. Unfortunately, differently from the electronic ground state which has a linear equilibrium geometry, many of the excited states are supposed to have a bent structure and their spectroscopic investigations are difficult since bent states show only weak features in the absorption spectra.

As a general agreement, in the energy region between 7 and 10 eV, seven electronic states are assumed to lie ( ${}^3\Sigma_u^+$ ,  ${}^{3,1}\Sigma_u^-$ ,  ${}^{3,1}\Delta_u$ ,  ${}^{3,1}\Pi_g$ ), while above 10 eV, the excitation spectrum is composed of several Rydberg series and Rathenau progressions [64, 65].

Itikawa [20] and Deschamps et al. [21] provide a review of the electronic excited state energies measured or calculated by different authors (see Table 7 in [20] and Table I in [21]). These energies are listed in Table 1. Deschamps reports the vertical excitation energies of CO<sub>2</sub> electronic excited states calculated by Winter et al. [55], England et al. [56], Spielfiedel et al. [57, 58], Buenker et al. [59] and Nakatsuji et al. [60]. Itikawa reports also the spectroscopic results of photoabsorption studies performed by Rabalais et al. [66] and Chan et al. [67] and the excitation energy employed in the cross-section calculation by Lee et al. [61].

The calculations of Nakatsuji et al. [60] are based on symmetry-adapted cluster (SAC) method with CI (SAC-CI) study. Nakatsuji et al. assumed a linear geometry, giving information about the possibility of bent geometry of some excited states by looking to the molecular orbital characteristics. The bent structure of the excited states of CO<sub>2</sub>, instead, was theoretically investigated by Spielfiedel et al. [57, 58] and by Buenker et al. [59]. Finally, we have added also the energies calculated by Mulligan [62] by LCAO-MO SCF method (Linear Combination of Atomic Orbitals Molecular Orbitals with the Roothaan's

**Table 1** CO<sub>2</sub> electronic excited states: calculated vertical excitation energies (a, b, c, d, e, i), energies derived from experiments (f, g) (photoabsorption studies), excitation energy employed in the cross-section calculations (h)

| Exc. state                               | Winter [55] <sup>a</sup> | England [56] <sup>b</sup> | Spiefie-<br>del [57,<br>58] <sup>c</sup> | Buenker [59] <sup>d</sup> | Nakatsuji<br>[60] <sup>e</sup> | Rabalais [66] <sup>f</sup> | Chan [67] <sup>g</sup> | Lee [61] <sup>h</sup> | Mulligan [62] <sup>i</sup> | Triana<br>EOM-<br>CCSD [63] <sup>i</sup> | Triana MRCI<br>[63] <sup>i</sup> |
|--|--------------------------|---------------------------|--|---------------------------|--------------------------------|----------------------------|------------------------|-----------------------|----------------------------|--|----------------------------------|
| <sup>1</sup> Π <sub>u</sub>              | 11.53                    | 11.45                     |  | 11.64                     | 11.39                          |                            | 11.28                  | 16.3                  |                            | 11.38                                    | 11.13                            |
| <sup>3</sup> Π <sub>u</sub>              | 11.49                    | 11.43                     |  |                           | 11.31                          |                            |                        | 16.3                  |                            |  |                                  |
| <sup>1</sup> Σ <sup>+</sup> <sub>u</sub> | 11.07                    | 11.20                     |  | 11.38                     | 11.00                          | 11.08                      | 10.3                   | 22.1                  |                            | 11.02                                    | 10.93                            |
| <sup>1</sup> Δ <sub>u</sub>              | 8.38                     | 9.43                      | 9.28                                     | 9.54                      | 9.32                           | 8.41                       | 8.38                   | 9.95                  |                            | 9.08                                     | 9.33                             |
| <sup>1</sup> Σ <sup>-</sup> <sub>u</sub> | 8.27                     | 9.42                      | 9.19                                     | 9.42                      | 9.27                           | 6.53                       |                        | 9.73                  |                            | 8.95                                     | 9.06                             |
| <sup>3</sup> Σ <sup>-</sup> <sub>u</sub> | 8.24                     | 9.42                      | 9.21                                     |                           | 9.19                           |                            |                        | 9.73                  |                            |  |                                  |
| <sup>1</sup> Π <sub>g</sub>              | 9.23                     | 9.10                      | 9.00                                     | 9.16                      | 8.93                           | 9.31                       | 9.30                   |                       |                            | 8.84                                     | 8.87                             |
| <sup>3</sup> Δ <sub>u</sub>              | 7.83                     | 9.02                      | 8.83                                     |                           | 8.80                           |                            |                        | 9.13                  |                            |  |                                  |
| <sup>3</sup> Π <sub>g</sub>              | 8.95                     | 8.86                      | 8.61                                     |                           | 8.73                           |                            |                        | 14.6                  |                            |  |                                  |
| <sup>3</sup> Σ <sup>+</sup> <sub>u</sub> | 7.35                     | 8.65                      | 8.35                                     |                           | 8.15                           | 4.89                       |                        | 8.53                  |                            |  |                                  |
| <sup>1</sup> Σ <sup>+</sup> <sub>0</sub> | 0.0                      | 0.0                       | 0.0                                      |                           |                                |                            |                        |                       |                            |  |                                  |



**Table 2** Available electron excitation cross sections from ground state

| Excited state                            | Mu-Tao [68] | Lee [61] | Kawahara [69] |
|--|-------------|----------|---------------|
| $X^1\Sigma_0^+ \rightarrow ^1\Pi_u$      | X           |          | X             |
| $X^1\Sigma_0^+ \rightarrow ^3\Pi_u$      | X           |          |               |
| $X^1\Sigma_0^+ \rightarrow ^1\Sigma_u^+$ | X           |          | X             |
| $X^1\Sigma_0^+ \rightarrow ^1\Delta_u$   | X           | X        |               |
| $X^1\Sigma_0^+ \rightarrow ^1\Sigma_u^-$ |             | X        |               |
| $X^1\Sigma_0^+ \rightarrow ^3\Sigma_u^-$ |             | X        |               |
| $X^1\Sigma_0^+ \rightarrow ^1\Pi_g$      | X           |          |               |
| $X^1\Sigma_0^+ \rightarrow ^3\Delta_u$   | X           | X        |               |
| $X^1\Sigma_0^+ \rightarrow ^3\Pi_g$      | X           |          |               |
| $X^1\Sigma_0^+ \rightarrow ^3\Sigma_u^+$ | X           | X        |               |

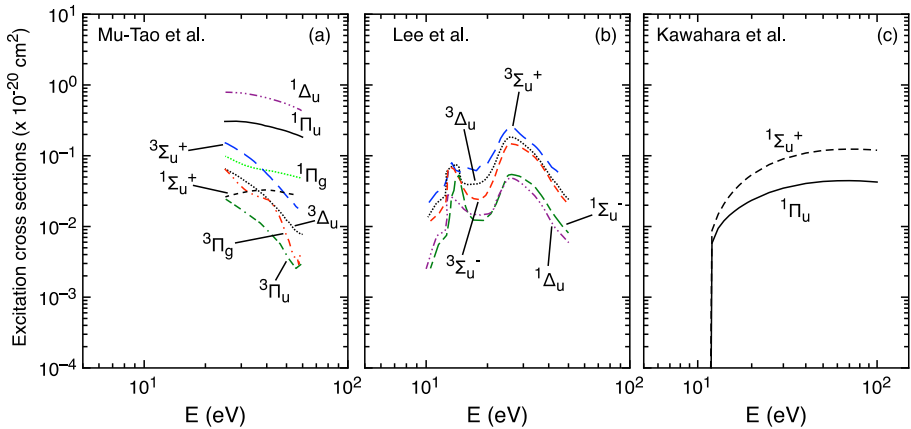


**Fig. 1** CO<sub>2</sub> electronic state excitation cross sections calculated by Mu-Tao et al. [68] for the  $^3,1\Sigma_u^+$ ,  $^3,1\Delta_u$ ,  $^3,1\Pi_u$ ,  $^3,1\Pi_g$ , Lee et al. [51] for the  $^3\Sigma_u^+$ ,  $^1\Delta_u$ ,  $^3\Delta_u$ ,  $^1\Sigma_u^-$ ,  $^3\Sigma_u^-$  states and those measured by Kawahara et al. [69] for  $^1\Pi_u$  and  $^1\Sigma_u^+$  states

Self-Consistent Field method) and the recent calculations by Triana et al. [63] by means of EOM-CCSD (Equation of Motion Coupled Cluster Singles and Doubles) and MRCI (Multi Reference Configuration Interaction) methods.

The available electron impact excitation cross sections for the listed CO<sub>2</sub> electronic excited states are reported in Table 2 and in Fig. 1. In particular, Mu-Tao and McKoy [68], by using a distorted-wave method, calculated the cross sections for the excitation of eight states for the energy range 25–60 eV. Unfortunately, this energy range is far from the threshold energies and cannot adequately describe the process. More recently, Lee et al. [61] have provided more energy extended cross sections (up to the threshold energies) for only five excited states by using a close-coupling method. Excitation cross sections for the  $^1\Sigma_u^+$  and  $^1\Pi_u$  states have been derived by Kawahara et al. [69] by means of cross-beam experiments [70]. These cross sections were also compared to integral cross sections calculated by using the BE f-scaling approach [71], generally used for electron impact excitation of dipole-allowed electronic states, finding a good agreement.

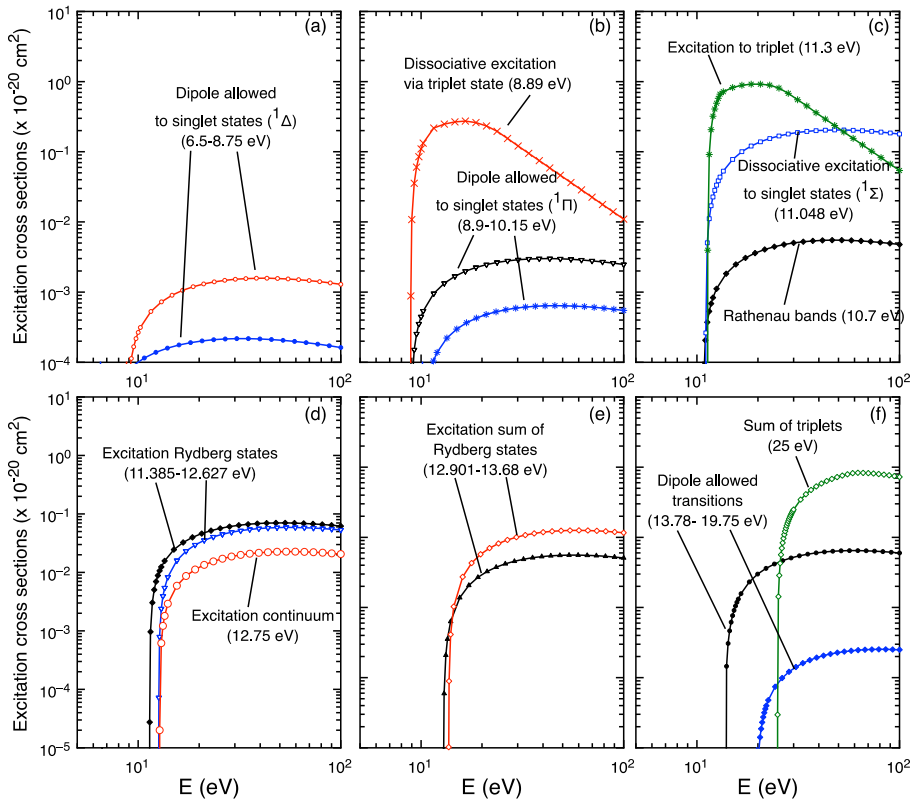


**Fig. 2** Selected electronic excitation cross sections of  $\text{CO}_2$  from the LXCat database Biagi-v7.1 [24]

Recently, data from Biagi's Magboltz code [23] were added to the LXCat database (Biagi-v7.1) [24]. The Biagi database contains several cross sections for the excitation of electronic excited states, which are assumed to be involved in dissociation (fully dissociative). These electronic excited state cross sections are derived mainly from the analysis of photoabsorption in  $\text{CO}_2$  [72]. This technique gives cross sections for levels that are coupled with the ground electronic state through dipole excitation. For non-dipole allowed transitions, called triplet excitations, the related cross sections are optimized in Magboltz [23] to reproduce the measured Townsend ionization coefficient [73]. The electronic excited state cross sections included in the Biagi database, covering the energy range 6.5–25 eV (65 cross sections) are the following and a selection of them is reported in Fig. 2:

- (1) Dipole allowed transitions to singlet states ( $^1\Delta$ ) leading to dissociation of  $\text{CO}_2$  into CO and O, described by 10 different cross sections with thresholds ranging between 6.5 and 8.75 eV.
- (2) Dissociative excitation via triplet state with threshold 8.89 eV.
- (3) Dipole allowed transitions to singlet states ( $^1\Pi$ ) leading to dissociation, described by 6 different cross sections with thresholds ranging between 8.9 and 10.15 eV.
- (4) Excitation Rathenau bands with threshold 10.7 eV.

- (5) Dissociative excitation to singlet ( $^1\Sigma$ ) with threshold 11.048 eV.
- (6) Dissociative excitation to triplet with threshold 11.3 eV.
- (7) Excitation Rydberg states, described by 11 different cross sections with thresholds from 11.385 to 12.627 eV.
- (8) Excitation continuum with threshold 12.75 eV
- (9) Excitation sum of Rydberg states, described by 7 different cross sections with thresholds from 12.901 to 13.68 eV
- (10) Dipole allowed transitions leading to dissociation, described by 25 different cross sections with threshold from 13.78 to 19.75 eV.
- (11) Dissociative excitation via sum of triplets with a threshold of 25 eV.

It should be noted that, in the case of swarm-derived cross section sets as most of the database available at the LXCat website, including the Biagi one, all the cross sections correspond to lumped processes describing generic excitation processes, where the individual processes are often not identified and the involved states cannot be correctly described by the standard notation for molecular excited states.

The highest excitation cross sections from the Biagi database reported in Fig. 2 are lower than  $10^{-20}$  cm<sup>2</sup> and of the same order of magnitude, near the threshold, of the 7 eV (dissociation) and 10.5 eV (electronic excitation) cross sections of the Phelps database.

The inclusion in the kinetics of the electronic excited states reported in Table 1 requires the implementation of appropriate kinetic equations for each of them, but, at the moment, the lack of reasonable electron impact cross sections, and the scarce information about radiative lifetimes and quenching rates prevent the direct inclusion of these states in the present model.

Another important difficulty is to understand which electronic excitation cross sections should be considered as already implicitly included in the electron impact dissociation cross section considered, and which of them, instead, can be added to the set of cross sections without overlapping. The Phelps and Biagi databases are based on swarm data analysis, and their dissociation cross sections could already include some electronic excitation cross sections. Following the consideration made by Polak [74] in the building up of his CO<sub>2</sub> dissociation cross section, one could reasonable think that the first seven excitation cross section related to the singlets ( $^1\Sigma_u^-$ ,  $^1\Pi_g$ ,  $^1\Delta_u$ ) and triplets ( $^3\Sigma_u^+$ ,  $^3\Sigma_u^-$ ,  $^3\Pi_g$ ,  $^3\Delta_u$ ) states could be considered as already included in the 7 eV cross section of the Phelps database.

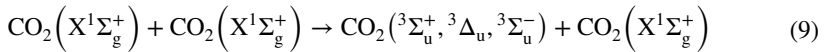
This approach has been used by Stankovic et al. [75]. They calculated electron impact ionization and electronic state excitation rate coefficients in non-equilibrium CO<sub>2</sub> plasma under time-dependent radio-frequency (RF) electric field with the eedf calculated by Monte Carlo (MC) simulations by including in the CO<sub>2</sub> cross section database:

- (1) the 7 eV excitation cross section taken from the Hake and Phelps database;
- (2) the two electronic excitation cross sections measured by Kawahara et al. [69] related to the states  $^1\Sigma_u^+$  and  $^1\Pi_u$ ;
- (3) a 10 eV excitation cross section (see also [76]).

The first seven electronic excited states excitation cross sections are assumed already included in the 7 eV cross section. The 10 eV cross section was calculated after subtraction of the summed cross sections for all scattering types they considered in the simulation (elastic scattering, excitation of different vibrational modes, electronic excitation and ionization) from the experimentally measured total cross sections given by Itikawa [20]

with an excellent agreement between their calculated transport coefficients and transport parameters measured by other authors.

Another attempt to include other CO<sub>2</sub> electronic excited states has been performed by Bultel et al. [77] in the development of a two-temperature collisional-radiative model “CoRaM-MARS” for the description of the nonequilibrium flows around a hypersonic vehicle entering the Martian atmosphere. They included in the CO<sub>2</sub> kinetic model only the triplet states  $^3\Sigma_u^+$ ,  $^3\Delta_u$ ,  $^3\Sigma_u^-$  and for such states they consider the electronic excitation processes under heavy particle impact of the kind



The correspondent rate coefficient was calculated by applying an analytical form [78].

## CO<sub>2</sub> Electron Impact Dissociation Model via Electronic Excitation

Particular attention in literature has been devoted to the identification of the CO<sub>2</sub> electron impact dissociation cross section [79–81], which is assumed to be implicitly included among the available electronic excitation cross sections.

In general, the 7 eV excitation cross section from Phelps [82, 83] with products  $CO(X) + O(^1D)$  is widely used in literature and seems to give reasonable CO<sub>2</sub> dissociation rates compatible with experiments in various conditions [79, 81]. The Phelps database provides also an electronic excitation cross section at 10.5 eV. This state, in general, is considered as a metastable state even though other authors [84] consider the possible dissociation via this state with products  $CO(a^3\Pi) + O(^3P)$ . Another possibility tested in literature [85] is the experimental dissociation cross section of Cosby [86], with an energy threshold of 12.5 eV, which provided lower electron impact dissociation rates respect to Phelps. Recently, Morillo-Candas et al. [80] showed that a better comparison with experimental CO<sub>2</sub> dissociation rates is obtained by using the Polak and Slovetsky’s cross section [74] for E/N in the range 45–105 Td. However, they still suggest the use of the 7 eV Phelps cross section for the calculation of the eedf through the Boltzmann equation to maintain the coherence and the consistency of the electron impact cross section dataset obtained by swarm analysis procedures.

For E/N values larger than 90 Td, instead, Babaeva et al. [87] suggested again the use of the Phelps dissociation cross sections, in particular the 10.5 eV one, in corona and dielectric-barrier discharges.

It is worth noticing that the dissociation through electronically excited states can also result from a vibrational-electronic (VE) transition mechanism, as that one reported in [88], where the rates for VE, VT and dissociation involving the  $^3B_2$  CO<sub>2</sub> excited state are estimated and the role of Franck Condon factors on VE rates is briefly discussed. This channel can contribute in enhancing the global dissociation rate of CO<sub>2</sub> and could be included in the present model in the future.

The availability of new electronic excited cross sections of the Biagi database which can be assumed as dissociative ones provides another possible model for describing electron impact CO<sub>2</sub> dissociation.

It should be noted, that the assumption of considering these states as fully dissociative ones is suggested from the analysis of photoabsorption spectra, which indicate that excitation to singlet and triplet states between 6 and 12 eV are related to fast processes like

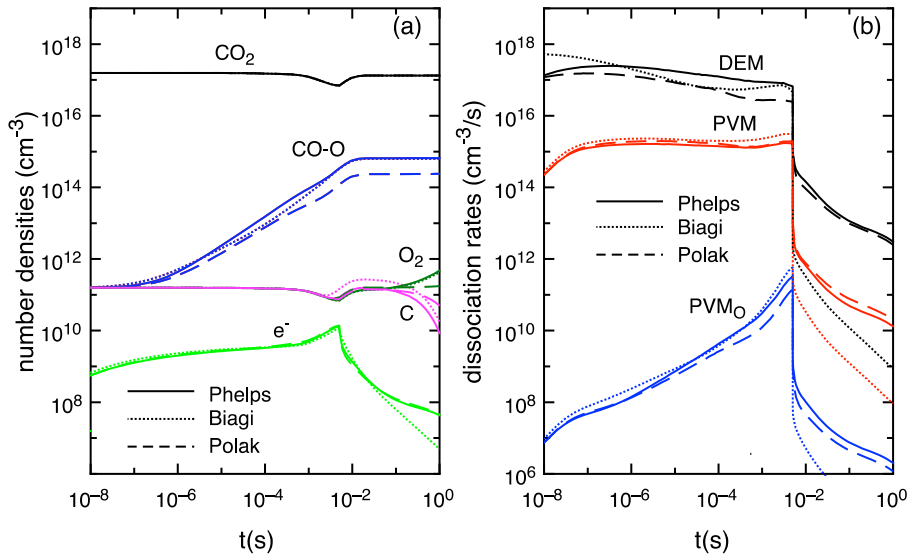


**Fig. 3** Time evolution of the number densities of the species and of the dissociation rates in glow discharge conditions ( $P=5$  torr,  $T_{\text{gas}}^{\text{exp}}(t)$ ,  $t_d=5$  ms,  $P_d=1$  W/ $\text{cm}^{-3}$ ) calculated with the dissociation model connected to the Phelps (full lines) and to the Biagi database (dotted lines). Dashed lines correspond to the results obtained by using the Polak and Slovetsky's dissociation cross section

dissociation. However, some uncertainties in the calculation of the corresponding dissociation rates are expected due to the unknown dissociation fraction of these electronically excited states, whose decay could occur also by different paths, for example vibrational relaxation, suggesting that further investigation on this point is still needed, as pointed out also by Vialetto [89].

In this section, we would like to test this new dissociation model, i.e. the Biagi one, and to compare the corresponding simulation results with the results obtained by the dissociation model linked to the Phelps database. The comparison has been made firstly in glow discharge conditions, in which  $\text{CO}_2$  dissociation occurs essentially by electron impact and the  $\text{CO}_2$  is characterized by low vibrational excitation, and then in MW discharge conditions in which vibrational excitation becomes more important for  $\text{CO}_2$  dissociation.

In the dissociation model associated to the Phelps database, the 7 eV electronic excitation cross section is considered as dissociative one, while the one at 10.5 eV is accounted for as an electronic excitation cross section. Moreover, the electron impact dissociation from vibrational excited levels is also accounted in the Phelps case by considering the same 7 eV dissociation cross section with a threshold shifting according to the vibrational energy.

In the Biagi dissociation model, we substitute the 7 and 10.5 eV electronic excitation cross sections with the electronic excitation cross sections taken from the Biagi database in the energy range 6.5–12 eV (65 cross sections) and listed in section “[CO<sub>2</sub> electronic excited states: a literature review](#)”. All these cross sections are taken as dissociative ones and in the lack of knowledge of the excited state electronic structure and envisaging the possibility of pre-dissociation mechanisms, the fragments CO and O are considered formed in their ground state.

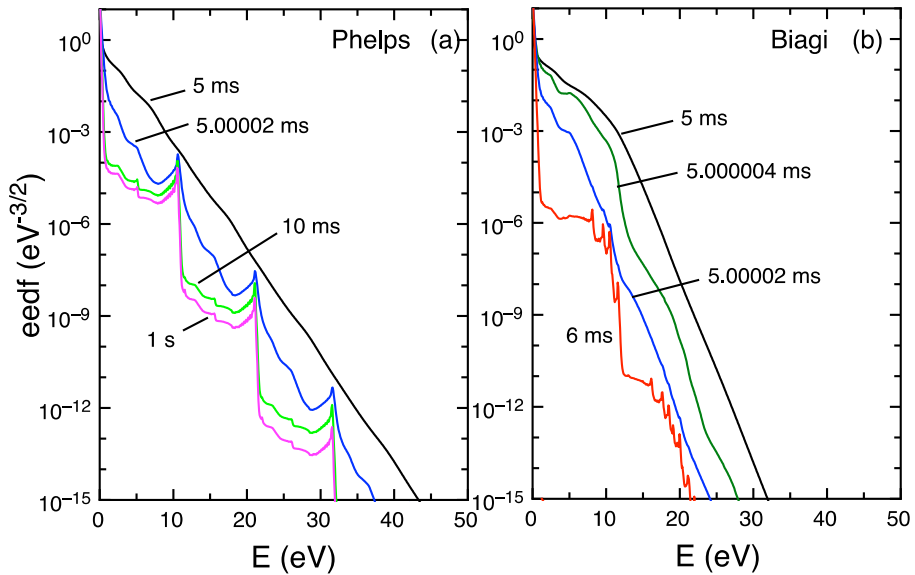


**Fig. 4** Eedf time evolution in the post-discharge calculated with the dissociation model based on the Phelps (a) and the Biagi database (b) in glow discharge conditions

At the moment, in the Biagi dissociation model, we have preferred not to add any scaled cross sections with the vibrational energy to test, as a first attempt, a pure dissociation model based only on the use of electronic excitation cross sections.

The glow discharge conditions chosen are the same as those reported by Grofulovich et al. [47] and by Klarenaar et al. [3] and already investigated in [46] ( $P=5$  torr,  $T_{\text{gas}}^{\text{exp}}(t)$ ,  $t_d=5$  ms,  $P_d=1$  Wcm $^{-3}$ ). In particular, the pressure  $P$  is kept constant during all the time evolution as well as the power density  $P_d$  during the discharge time  $t_d$ , while the gas temperature follows the time dependent profile  $T_{\text{gas}}^{\text{exp}}(t)$  derived from experiments, i.e. it increases from 300 K up to nearly 700 K for  $t < t_d$ , while it decreases to 300 K in the post-discharge for  $t > t_d$  (see Fig. 2a in [46]). In the post-discharge, i.e. for  $t > t_d$ ,  $P_d=0$  ( $E/N=0$ ). Figure 3 shows the time evolution of number densities of the species and of the dissociation rates in these glow discharge conditions in the two dissociation models. In these conditions,  $\text{CO}_2$  dissociation occurs essentially by electron impact, i.e. CO and O number densities follow the same time dependent profile (Fig. 3a) and DEM rates are higher than the others (Fig. 3b). The use of the Biagi dataset does not change global number densities respect to the Phelps case both in discharge and post-discharge, showing comparable results with the Phelps database (Fig. 3a). Calculated dissociation rates in the Biagi and Phelps case are nearly the same in discharge conditions, while some differences are registered for DEM and PVM rates especially in post-discharge conditions due to differences in the eedf time evolution. In Fig. 3 we have also reported the results obtained by using the Polak and Slovetsky's cross section for dissociation. The use of this cross section, instead, leads to lower CO–O density and lower DEM rates respect to the Biagi and Phelps case. These results are compatible to those shown by Vialetto et al. [89], who compared electron impact dissociation rates calculated by Monte Carlo Flux and Bolsig $^+$  codes by using both the Biagi and Polak and Slovetsky's cross sections as a function of the reduced electric field in the same glow discharge conditions. They showed that the rates obtained in the

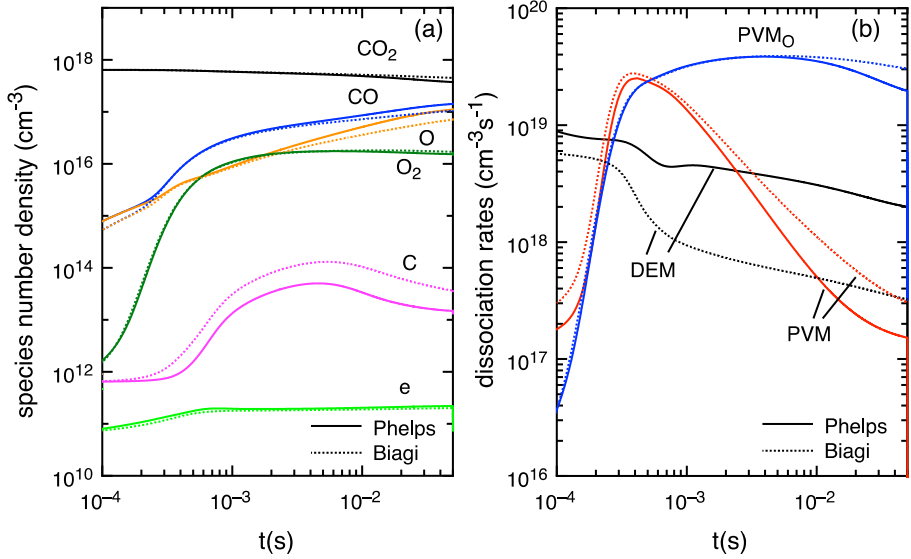


**Fig. 5** Time evolution of the number densities of the species and of the dissociation rates in MW discharge conditions ( $P=20$  torr,  $T_{\text{gas}}=300$  K,  $t_d=50$  ms,  $P_d=80$  W/cm<sup>-3</sup>) calculated with the dissociation model connected to the Phelps (full lines) and to the Biagi database (dotted lines)

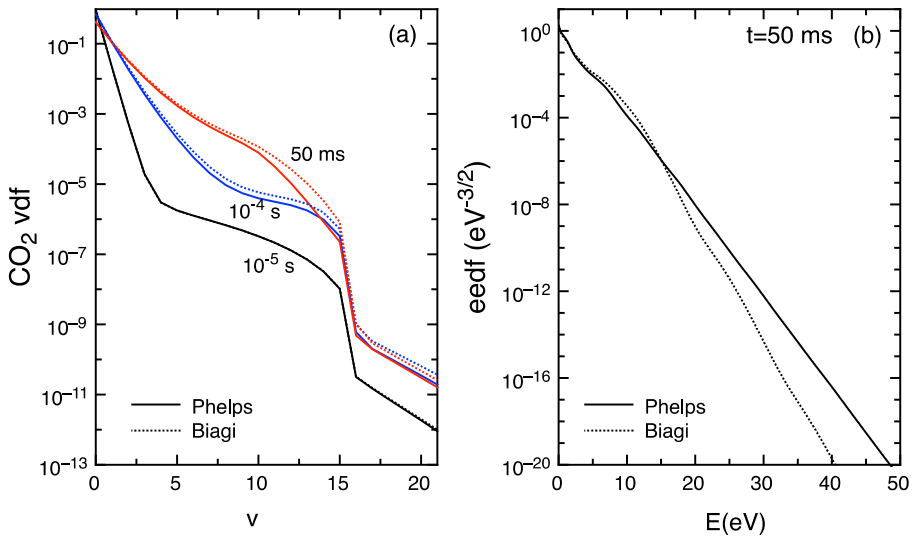


**Fig. 6 a** CO<sub>2</sub> vdf time evolution and **b** stationary eedf ( $t=t_d=50$  ms) in MW discharge conditions ( $P=20$  torr,  $T_{\text{gas}}=300$  K,  $t_d=50$  ms,  $P_d=80$  W/cm<sup>-3</sup>) calculated with the dissociation model connected to the Phelps (full lines) and to the Biagi database (dotted lines)

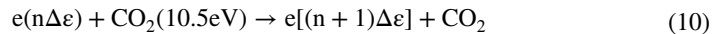
case of Biagi and Polak and Slovetsky are quite compatible for  $E/N < 60$  Td, while for higher  $E/N$ , those of Polak and Slovetsky are lower than those of the Biagi ones.

Stationary eedf in discharge ( $t = t_d = 5$  ms) and its time evolution in the post-discharge is shown in Fig. 4.

As it can be seen, in both cases, the eedf evolves towards a non-equilibrium distribution characterized by the presence of characteristic peaks due to superelastic collisions, which have a physical explanation. The two-term Boltzmann equation, in fact, allows discontinuities also in the presence of continuous cross sections because of the source terms due to inelastic and superelastic collisions (see Eq. 1) [29]. In particular, the effect of electronic superelastic collisions is to reproduce (approximately) at the threshold energy ( $E_{thr}$ ) the eedf distribution scaled by the population of the electronically excited state, with no contribution for  $E < E_{thr}$  [90]. Therefore, in the short time, the distribution presents a peak at the threshold energy and a hole for lower values. The hole is filled in the long time by elastic collisions. If the superelastic collisions are strong enough, the peak structure remains visible as it happens in the present conditions. Especially in the post-discharge, the peaks due to the products of  $CO_2$  dissociation ( $O_2$ ,  $O$ ,  $C$ ) could be also visible characterizing the shape of the eedf.

The eedf calculated with the Biagi dataset has lower populated high energy tails due to the presence in the database of dissociation cross sections by electronic excitation with high threshold energies.

Moreover, the eedf does not present the characteristic peaks at energies 10.5 eV and multiple of that as in the case of the Phelps database which are due to the superelastic electronic collisions involving the electronic excited state  $CO_2$  (10.5 eV), i.e. the processes of the kind



with  $n=0, 1, 2$ , etc. and  $\Delta\varepsilon = 10.5$  eV.

Some superelastic electronic peaks around 10 eV (and multiple) appears in the Biagi database case (see Fig. 4b) at stationary conditions due to electronic excited states of O atoms ( $O(^3S^0)$ ,  $O(^5S^0)$ ).

Such differences in the eedf and in the calculated dissociation rates in the post-discharge, however, do not influence global  $CO_2$  density since the low electron density and electron temperature conditions make dissociation practically absent in the post-discharge.

Figure 5, instead, shows the time evolution of the densities of the species and of the dissociation rates in MW discharge conditions characterized by  $P=20$  torr,  $T_{gas}=300$  K,  $t_d=50$  ms,  $P_d=80$  Wcm<sup>-3</sup>, in the two dissociation models. In these conditions, the pressure  $P$  and the gas temperature  $T_{gas}$  are kept constant as well as the power density  $P_d$  during the residence time  $t_d$  in the discharge, while for  $t > t_d$ ,  $P_d=0$  ( $E/N=0$ ). Globally, the species densities behavior is similar even if a slightly decrease of  $CO_2$  dissociation is predicted when the dissociation model linked to the Biagi database is used. This is essentially due to the lack in the Biagi dissociation model of electron impact dissociation processes from  $CO_2$  vibrationally excited states (see Eq. (5)) which, in this case, differently from the glow discharge case, have a more important impact in the global dissociation of  $CO_2$  due to a higher  $CO_2$  vibrational excitation. The corresponding  $CO_2$  vdf in the case of Phelps has slightly underpopulated upper energy tail due to the account of these processes and the corresponding PVM rates are lower respect to the Biagi case (see Fig. 5b). The inclusion of higher threshold energy dissociation cross section in the Biagi database underpopulates the eedf at higher energies respect to the Phelps model (see Fig. 6a) reducing the importance of electron impact dissociation processes with predicted lower DEM rates in the Biagi case as it can be seen in Fig. 5b.



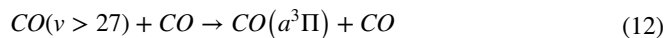
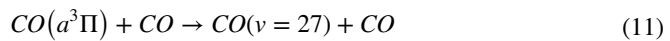
**Table 3** Kinetic processes involving the  $\text{CO}(a^3\Pi)$  electronic excited state: old kinetic scheme

|   | Process  | Cross sect/rate coeff                  | References |
|---|--|--|------------|
| 1 | $e + \text{CO}(X) \rightarrow e + \text{CO}(a^3\Pi)$                         | Cross sect                             | [100]      |
| 2 | $\text{CO}(a^3\Pi) + \text{CO} \rightarrow \text{CO}(X, v = 27) + \text{CO}$ | $10^{-10} \text{ cm}^3 \text{ s}^{-1}$ | [25]       |
| 3 | $\text{CO}(X, v > 27) + \text{CO} \rightarrow \text{CO}(a^3\Pi) + \text{CO}$ | $10^{-13} \text{ cm}^3 \text{ s}^{-1}$ | [101, 102] |
| 4 | $\text{CO}(a'^3\Sigma^+) \rightarrow \text{CO}(a^3\Pi) + h\nu_1$             | $10^4 \text{ s}^{-1}$                  | [103, 104] |
| 5 | $\text{CO}(b^3\Sigma^+) \rightarrow \text{CO}(a^3\Pi) + h\nu_2$              | $1.852 \cdot 10^7 \text{ s}^{-1}$      | [103, 105] |
| 6 | $\text{CO}(a^3\Sigma^+) \rightarrow \text{CO}(X^1\Sigma^+) + h\nu_3$         | $133 \text{ s}^{-1}$                   | [106]      |

These results show that, in conditions characterized by low vibrational excitation and in which electron impact dissociation dominates the kinetics as glow discharges, the Biagi database provide same  $\text{CO}_2$  dissociation rates as Phelps ones. This is the result of the compatibility of the two different datasets which have been built up by using swarm analysis procedure. However, in conditions in which vibrational excitation becomes important, lower  $\text{CO}_2$  conversion rate are obtained with the dissociation model connected to the Biagi dataset since only dissociation from electronic excited states is accounted for without modeling electron dissociation from vibrational excited states (see Eq. (5)). Further studies of this particular aspect are necessary, since an integration of the proposed model connected with the Biagi dataset should be performed to take into account also the latter processes.

### A Focus on $\text{CO}(a^3\Pi)$ Kinetics

The first electronic excited state of the CO molecule, i.e.  $\text{CO}(a^3\Pi)$ , is a metastable state at 6 eV with a radiative lifetime  $\sim 2.6$  ms [91, 92]. Besides affecting the eedf through super-elastic collisions, according to Porshnev [25], it affects also the corresponding CO ground state vdf by means of the following quenching and vibrational-electronic (VE) transitions



The quenching process in Eq. (11) creates a well-defined peak at  $v=27$ , as shown in [33–35], progressively rounded off by VV and VT collisions. Moreover, the  $\text{CO}(a^3\Pi)$  state is involved in chemical reactions, which contribute to  $\text{CO}_2$  dissociation/recombination. Recently, its role on the  $\text{CO}_2$  dissociation mechanisms was investigated in DC glow discharge conditions characterized by pressure from 0.4 to 5 Torr [93–95] and also by Cenian et al. [96] in similar working conditions. They showed that the  $\text{CO}(a^3\Pi)$ , depending on the CO and  $\text{O}_2$  density, can either enhance the dissociation of  $\text{CO}_2$  or stimulates the reversion back to  $\text{CO}_2$ . Actually, the energy of this state (6 eV) is enough to dissociate  $\text{CO}_2$  and  $\text{O}_2$  molecules with rate coefficients close to the gas kinetic collision frequencies. In particular, in [93, 94], it is shown that, for gas mixtures with large amount of  $\text{CO}_2$  but low CO density, the reaction  $\text{CO}(a^3\Pi) + \text{CO}_2 \rightarrow 2\text{CO} + \text{O}$  contributes to enhance the dissociation. On the contrary, if the concentrations of CO and  $\text{O}_2$  are larger, the processes

**Table 4** New kinetic scheme for the  $\text{CO}(a^3\Pi)$  electronic excited state

|    | Process  | Cross sect/rate coeff                            | Branching ratio | References      |
|----|--|--|-----------------|-----------------|
| 1  | $e + \text{CO}(X) \rightarrow e + \text{CO}(a^3\Pi)$                         | Cross sect                                       |                 | [100]           |
| 2  | $\text{CO}(a^3\Pi) + \text{CO} \rightarrow \text{CO}(X, v = 27) + \text{CO}$ | $10^{-10} \text{ cm}^3 \text{ s}^{-1}$           | 0.984           | [25]            |
| 3  | $\text{CO}(X, v > 27) + \text{CO} \rightarrow \text{CO}(a^3\Pi) + \text{CO}$ | $10^{-13} \text{ cm}^3 \text{ s}^{-1}$           |                 | [101, 102]      |
| 4  | $\text{CO}(a'^3\Sigma^+) \rightarrow \text{CO}(a^3\Pi) + h\nu_1$             | $10^4 \text{ s}^{-1}$                            |                 | [103, 104]      |
| 5  | $\text{CO}(b^3\Sigma^+) \rightarrow \text{CO}(a^3\Pi) + h\nu_2$              | $1.852 \cdot 10^7 \text{ s}^{-1}$                |                 | [103, 105]      |
| 6  | $\text{CO}(a^3\Pi) \rightarrow \text{CO}(X^1\Sigma^+) + h\nu_3$              | $133 \text{ s}^{-1}$                             |                 | [106]           |
|    | Production processes   |  |                 |                 |
| 7  | $e + \text{CO}_2 \rightarrow e + \text{CO}(a^3\Pi) + \text{O}$               | Cross sect                                       |                 | [107]           |
| 8  | $e + \text{CO}_2^+ \rightarrow \text{CO}(a^3\Pi) + \text{O}$                 | $3 \cdot 10^{-7} \text{ cm}^3 \text{ s}^{-1}$    |                 | [106, 108, 109] |
|    | Loss or quenching processes  |  |                 |                 |
| 9  | $\text{CO}(a^3\Pi) + \text{O}_2 \rightarrow \text{CO} + \text{O}_2$          | $6 \cdot 10^{-11} \text{ cm}^3 \text{ s}^{-1}$   | 0.4             | [95, 110, 111]  |
| 10 | $\text{CO}(a^3\Pi) + \text{O}_2 \rightarrow \text{CO} + 2\text{O}$           | $6 \cdot 10^{-11} \text{ cm}^3 \text{ s}^{-1}$   | 0.4             | [95, 110, 111]  |
| 11 | $\text{CO}(a^3\Pi) + \text{O}_2 \rightarrow \text{CO}_2 + \text{O}$          | $6 \cdot 10^{-11} \text{ cm}^3 \text{ s}^{-1}$   | 0.2             | [95, 110, 111]  |
| 12 | $\text{CO}(a^3\Pi) + \text{CO}_2 \rightarrow \text{CO} + \text{CO}_2$        | $10^{-11} \text{ cm}^3 \text{ s}^{-1}$           | 0.5             | [95, 106]       |
| 13 | $\text{CO}(a^3\Pi) + \text{CO}_2 \rightarrow 2\text{CO} + \text{O}$          | $10^{-11} \text{ cm}^3 \text{ s}^{-1}$           | 0.5             | [95, 106]       |
| 14 | $\text{CO}(a^3\Pi) + \text{O} \rightarrow \text{CO} + \text{O}$              | $1.9 \cdot 10^{-10} \text{ cm}^3 \text{ s}^{-1}$ |                 | [112]           |
| 15 | $\text{CO}(a^3\Pi) + \text{CO} \rightarrow \text{CO}_2 + \text{C}$           | $10^{-10} \text{ cm}^3 \text{ s}^{-1}$           | 0.016           | [95, 101, 111]  |

$\text{CO}(a^3\Pi) + \text{O}_2 \rightarrow \text{CO}_2 + \text{O}$  and  $\text{CO}(a^3\Pi) + \text{CO} \rightarrow \text{CO}_2 + \text{C}$  are prevailing and leads to the  $\text{CO}_2$  reversion [97, 98].

Thus, the  $\text{CO}(a^3\Pi)$  appears to be a key species in  $\text{CO}_2$  plasma dynamics and its kinetics needs further investigation with a more detailed kinetic description. Unfortunately, its direct measurement is very challenging and has been done only in very diluted gas mixture for  $\text{CO}_2$  laser study [99].

### New and Old Kinetic Schemes for $\text{CO}(a^3\Pi)$

The kinetics of the  $\text{CO}(a^3\Pi)$  was already studied in [33–35] by taking into account the processes listed in Table 3.

An important improvement of the  $\text{CO}(a^3\Pi)$  kinetics is proposed by including also new processes of production and loss. The new kinetic scheme is shown in Table 4. As new production processes, we have added the dissociative excitation of  $\text{CO}_2$  by electron impact ( $> 11.5 \text{ eV}$ ) (process 7), with the cross section measured by Wells et al. [107] by means of time-of-flight spectra and the dissociative recombination of  $\text{CO}_2^+$  ion (process 8), whose rate was suggested by [106], according also to measurements performed in the downstream of a MW plasma by [108, 109]. The new loss processes are quenching processes to the ground state in collisions with  $\text{O}_2$  (processes 9–10) and reactive quenching by collisions with  $\text{O}_2$  leading to dissociation into  $\text{CO}_2 + \text{O}$  (process 11), quenching to the ground state in collisions with  $\text{CO}_2$  (processes 12–13), quenching to the ground state in collisions with  $\text{O}$  (process 14) and reactive quenching by collisions with  $\text{CO}$  with dissociation into  $\text{C} + \text{CO}_2$  (process 15).

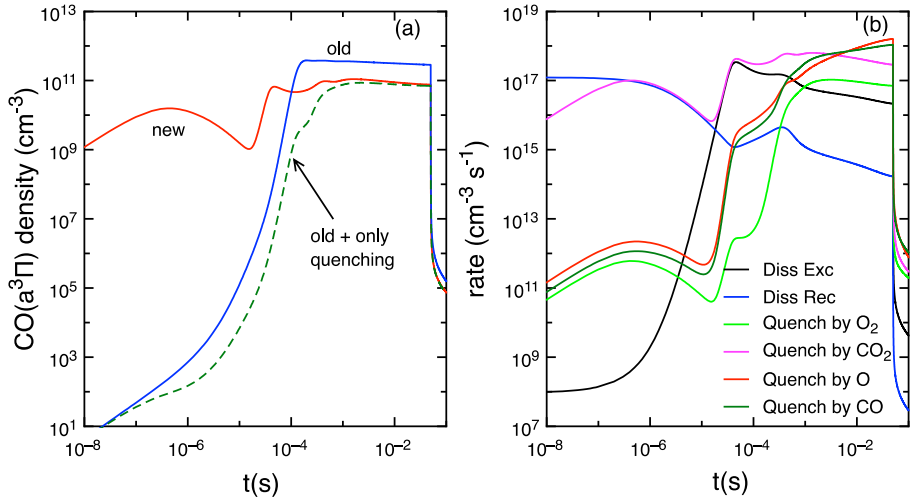


**Fig. 7** Time evolution of the **a**  $\text{CO}(a^3\Pi)$  number density and **b** rates ( $\text{cm}^{-3} \text{s}^{-1}$ ) of dissociative excitation (process 7), dissociative recombination (process 8), quenching by  $\text{O}_2$  (process 9–11), by  $\text{CO}_2$  (process 12–13), by  $\text{O}$  (process 14), by  $\text{CO}$  (process 15) (see Table 4) in the MW test case ( $T_{\text{gas}} = 300 \text{ K}$ ,  $P = 20 \text{ Torr}$ ,  $P_d = 80 \text{ Wcm}^{-3}$ ,  $t_d = 50 \text{ ms}$ )

### $\text{CO}(a^3\Pi)$ Kinetics Results

The new kinetic scheme was tested in the MW discharge conditions characterized by  $T_{\text{gas}} = 300 \text{ K}$ ,  $P = 20 \text{ Torr}$ ,  $P_d = 80 \text{ Wcm}^{-3}$ ,  $t_d = 50 \text{ ms}$ . In these calculations, the Phelps database is used. The following figures show what happens when, for the  $\text{CO}(a^3\Pi)$  kinetics, we use the old kinetic scheme (old), the old kinetic scheme with the adding of only the quenching processes 9–15 in Table 4 (old+only quenching) and finally the complete new kinetic scheme (new), with the addition also of the new production terms 7–8.

Figure 7 shows the time evolution of the  $\text{CO}(a^3\Pi)$  density in the three different kinetic schemes (old, old+only quenching, new) and of the rates ( $\text{cm}^{-3} \text{s}^{-1}$ ) of the new processes added to the  $\text{CO}(a^3\Pi)$  kinetics.

It is clear that by adding to the old kinetic scheme only the quenching processes (old+only quenching), the  $\text{CO}(a^3\Pi)$  state is globally less populated, while the insertion also of the new production terms, i.e. processes 7–8 in Table 4 (new), increases the  $\text{CO}(a^3\Pi)$  population essentially in the initial temporal range up to  $10^{-4} \text{ s}$ . In the microsecond time range, instead, the  $\text{CO}(a^3\Pi)$  population density, is equal to that one predicted by adding only the quenching processes.

By looking to the time evolution of the rates in Fig. 7b, it can be deduced that the new production and quenching terms act in different temporal ranges. The  $\text{CO}(a^3\Pi)$  population kinetics is dominated by the dissociative recombination process up to  $10^{-5} \text{ s}$ , due to its high rate coefficient, and by the quenching by  $\text{CO}_2$  due to the high  $\text{CO}_2$  concentration. After that, up to  $10^{-4} \text{ s}$ , also the dissociative excitation process becomes important in the production of  $\text{CO}(a^3\Pi)$  state due to the increase of its corresponding rate coefficient in time. For  $t > 10^{-4} \text{ s}$  up to the end of the pulse ( $t = 50 \text{ ms}$ ), quenching processes dominate the  $\text{CO}(a^3\Pi)$  kinetics, with an order of importance correlated to the concentration of the colliding partner, i.e. the kinetic is dominated by the quenching by  $\text{CO}_2$  for  $10^{-4} \text{ s} < t < 5$

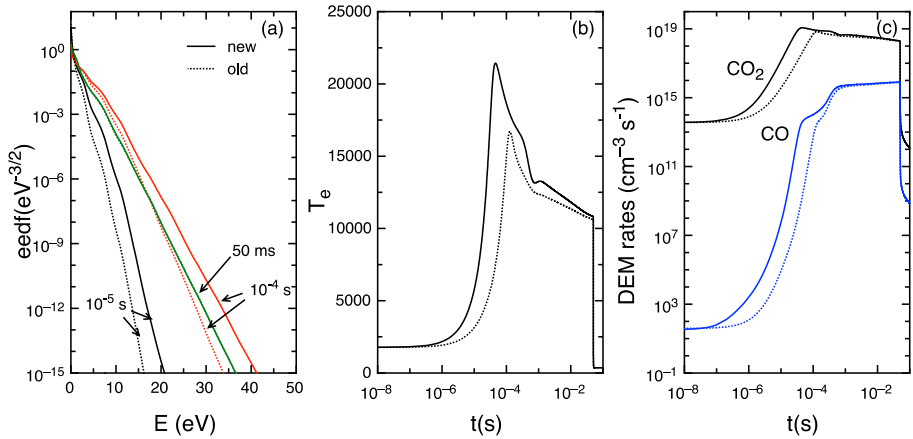


**Fig. 8** **a** Eedf time evolution during the discharge **b** electron temperature time evolution **c**  $\text{CO}_2$  and CO DEM rates ( $\text{cm}^{-3} \text{s}^{-1}$ ) in the old (dashed lines) and new (full lines) kinetic schemes in the MW test case ( $T_{\text{gas}} = 300 \text{ K}$ ,  $P = 20 \text{ Torr}$ ,  $P_d = 80 \text{ W cm}^{-3}$ ,  $t_d = 50 \text{ ms}$ )

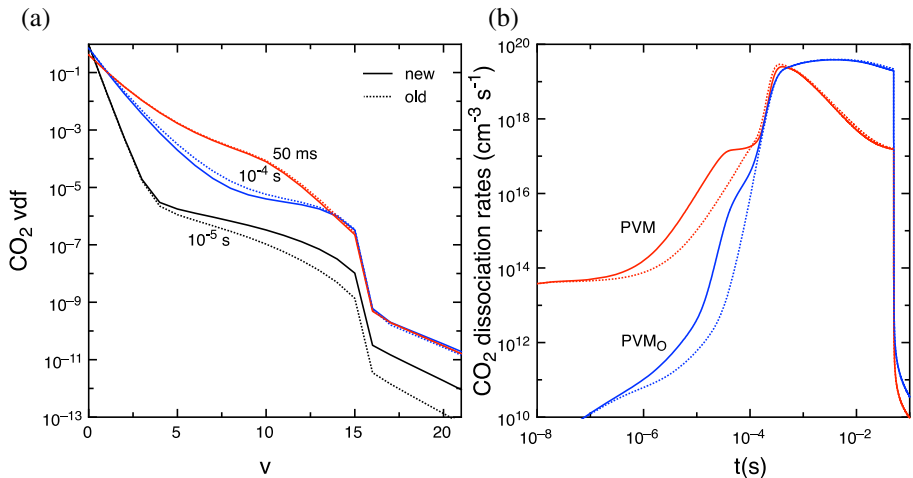


**Fig. 9** **a**  $\text{CO}_2$  vdf during the discharge; **b** PVM and  $\text{PVM}_O$  rates in the old (dashed lines) and new (full lines) kinetic schemes for the  $\text{CO}(a^3\Pi)$  in the MW test case ( $T_{\text{gas}} = 300 \text{ K}$ ,  $P = 20 \text{ Torr}$ ,  $P_d = 80 \text{ W cm}^{-3}$ ,  $t_d = 50 \text{ ms}$ , optically thin plasma)

$10^{-3}$ , and by the quenching by CO and O, for  $5 \cdot 10^{-3} \text{ s} < t < 50 \text{ ms}$ . In the post-discharge, production rates strongly decrease due to the decrease of the electron density, as well as the quenching rates.

The use of the new  $\text{CO}(a^3\Pi)$  kinetic scheme in the MW test case has some effects in the global kinetic of  $\text{CO}_2$  reactive plasma but only in the temporal range up to  $10^{-4} \text{ s}$ , i.e. in the range in which the production of  $\text{CO}(a^3\Pi)$  is increased by the dissociative excitation and dissociative recombination processes. In the microsecond range, the global kinetic remains more or less the same. Here the list of the changes:

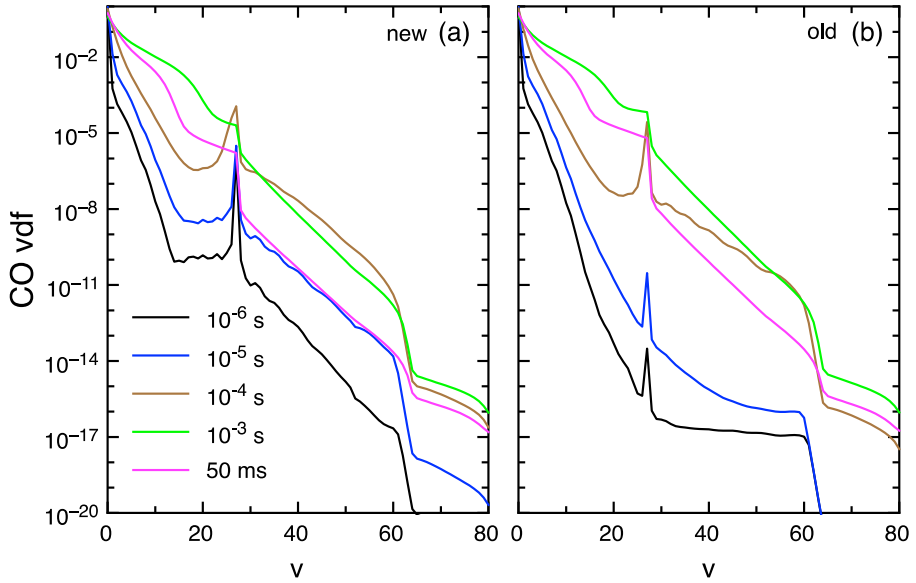


**Fig. 10** CO vdf time evolution in the **a** new and **b** old kinetic schemes during the discharge in the MW test case ( $T_{\text{gas}}=300\text{ K}$ ,  $P=20\text{ Torr}$ ,  $P_d=80\text{ Wcm}^{-3}$ ,  $t_d=50\text{ ms}$ )

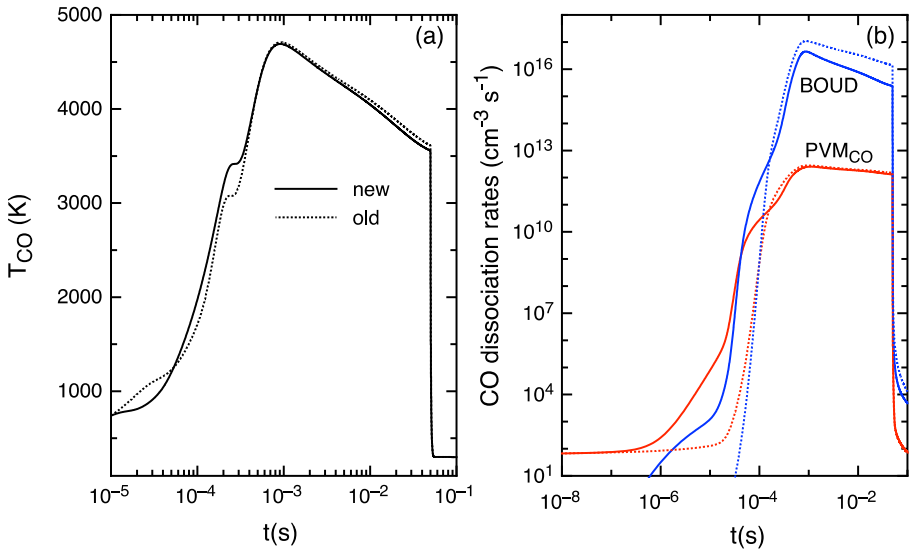


**Fig. 11** Time evolution of the **a** CO vibrational temperature and of the **b** CO dissociation rates by  $\text{PVM}_{\text{CO}}$ , i.e.  $\text{CO} + \text{M} \rightarrow \text{C} + \text{O} + \text{M}$  and by the Boudouard process, i.e.  $\text{CO}(v) + \text{CO}(w) \rightarrow \text{CO}_2(v) + \text{C}$ , in the new and old kinetic schemes during the discharge of the MW test case ( $T_{\text{gas}}=300\text{ K}$ ,  $P=20\text{ Torr}$ ,  $P_d=80\text{ Wcm}^{-3}$ ,  $t_d=50\text{ ms}$ )

**Fig. 12**  $\text{CO}_2$  and CO densities in the new (full lines) and old (dashed lines) kinetic schemes in the MW test case ( $T_{\text{gas}} = 300 \text{ K}$ ,  $P = 20 \text{ Torr}$ ,  $P_d = 80 \text{ Wcm}^{-3}$ ,  $t_d = 50 \text{ ms}$ )

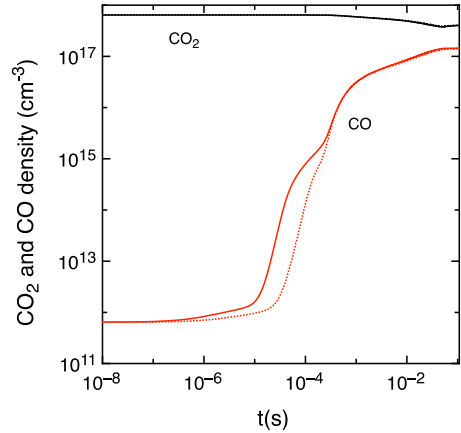


**Table 5**  $\text{CO}_2$  production and loss processes included in the kinetics

| Process  | Label                               |
|--|-------------------------------------|
| Loss   |                                     |
| $e + \text{CO}_2 \rightarrow e + \text{CO} + \text{O}$                                   | DEM                                 |
| $\text{CO}_2(\text{v}) + \text{M} \rightarrow \text{CO} + \text{O} + \text{M}$           | PVM                                 |
| $\text{CO}_2(\text{v}) + \text{O} \rightarrow \text{CO} + \text{O}_2$                    | $\text{PVM}_{\text{O}}$             |
| $\text{CO}(\text{a}^3\Pi) + \text{CO}_2 \rightarrow 2\text{CO} + \text{O}$               | Quench by $\text{CO}_2$             |
| Production   |                                     |
| $\text{CO} + \text{O} + \text{M} \rightarrow \text{CO}_2 + \text{M}$                     | $\text{REC}_{\text{CO-O}}$          |
| $\text{CO}(\text{v}) + \text{O}_2 \rightarrow \text{CO}_2 + \text{O}$                    | $\text{REC}_{\text{O}_2\text{-CO}}$ |
| $\text{CO}(\text{v}) + \text{CO}(\text{w}) \rightarrow \text{CO}_2(\text{v}) + \text{C}$ | Boud                                |
| $\text{CO}(\text{a}^3\Pi) + \text{O}_2 \rightarrow \text{CO}_2 + \text{O}$               | Quench by $\text{O}_2$              |
| $\text{CO}(\text{a}^3\Pi) + \text{CO} \rightarrow \text{CO}_2 + \text{C}$                | Quench by CO                        |

- (1) Eedf, electron temperature and  $\text{CO}_2$  and CO electron impact dissociation rates (DEM rates)

The higher  $\text{CO}(\text{a}^3\Pi)$  number density up to  $10^{-4} \text{ s}$  in the new kinetic scheme (see Fig. 8a) pumps the eedf towards higher energies respect to the old case by means of the superelastic electronic process involving the  $\text{CO}(\text{a}^3\Pi)$ , i.e.  $e(n\Delta\varepsilon) + \text{CO}(\text{a}^3\Pi) \rightarrow e((n+1)\Delta\varepsilon) + \text{CO}(0)$  with  $n=0, 1, 2, \text{ etc.}$  and  $\Delta\varepsilon = 6 \text{ eV}$ , increasing the electron temperature (see Fig. 8b) and also  $\text{CO}_2$  and CO electron impact dissociation (DEM) rates (see Fig. 8c) up to  $10^{-4} \text{ s}$ .

- (2)  $\text{CO}_2$  vdf and  $\text{CO}_2$  vibrational-induced dissociation rates (PVM)

The change in the eedf indirectly affects also the  $\text{CO}_2$  vdf by means of eV collisions: the overpopulation of the eedf at higher energies, in the new kinetic scheme and up to  $10^{-4} \text{ s}$ , pumps more energy to the vibrational energy levels in the higher-energy range, increasing the corresponding vdf tails and promoting  $\text{CO}_2$  dissociation from upper levels. This is confirmed by looking to Fig. 9 which shows the  $\text{CO}_2$  vdf in the two kinetic schemes during the discharge (Fig. 9a) and the time evolution of  $\text{CO}_2$  vibrational-induced dissociation rates of the processes in Eq. (6) (PVM) and (7) ( $\text{PVM}_{\text{O}}$ ) (Fig. 9b).

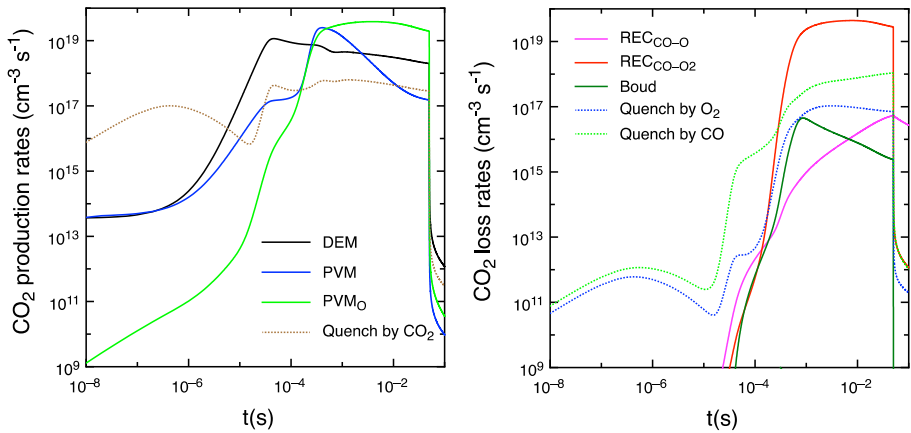


**Fig. 13**  $\text{CO}_2$  production and loss rates ( $\text{cm}^{-3} \text{s}^{-1}$ ) in the MW test case ( $T_{\text{gas}}=300 \text{ K}$ ,  $P=20 \text{ Torr}$ ,  $P_d=80 \text{ Wcm}^{-3}$ ,  $t_d=50 \text{ ms}$ )

The low-energy part of the  $\text{CO}_2$  vdf is not affected by the change of the kinetic scheme and as a consequence no effect on the  $\text{CO}_2$  vibrational temperature is observed.

(3) CO vdf, CO vibrational temperature and CO vibrational-induced dissociation rates

For the CO system, in addition to the indirect effect through eV processes (see previous point 2), also a direct effect on the CO vdf is present. The CO vdf is affected by the quenching process 2 (see Table 3 and 4) which induces a transfer of energy from  $\text{CO}(a^3\Pi)$  to the vibrational  $v=27$  level, creating a well distinct peak in the CO vdf. Figure 10 shows the comparison of the CO vdf in discharge conditions in the two kinetic schemes. The greatest differences occur again up to  $10^{-4} \text{ s}$  with the formation of higher peaks at  $v=27$  in the new kinetic scheme respect to the old one. An increase of the CO vibrational temperature of nearly 500 K up to  $10^{-4} \text{ s}$  is also registered together with an increase of the CO vibrational induced dissociation rates of the processes  $\text{CO} + \text{M} \rightarrow \text{C} + \text{O} + \text{M}$  ( $\text{PVM}_{\text{CO}}$ ) and of the Boudouard ones  $\text{CO}(v) + \text{CO}(w) \rightarrow \text{CO}_2(v) + \text{C}$  (Boud) (see Fig. 11).

(4)  $\text{CO}_2$  dissociation

Figure 12 shows the  $\text{CO}_2$  and CO number densities time evolution in the new and old kinetic scheme for  $\text{CO}(a^3\Pi)$ . As expected, CO production is slightly increased in the new kinetic scheme up to  $10^{-4} \text{ s}$ . This increase is due to the observed DEM and PVM rate increase (see Figs. 9c and 10b, respectively) in the same time range. In the ms time range, instead, the CO production does not change between the new and the old kinetic scheme because  $\text{CO}_2$  dissociation is essentially due to vibrational induced dissociation channels and the introduction of the production and quenching processes involving the  $\text{CO}(a^3\Pi)$ ,  $\text{CO}_2$  and CO does not affect the composition.

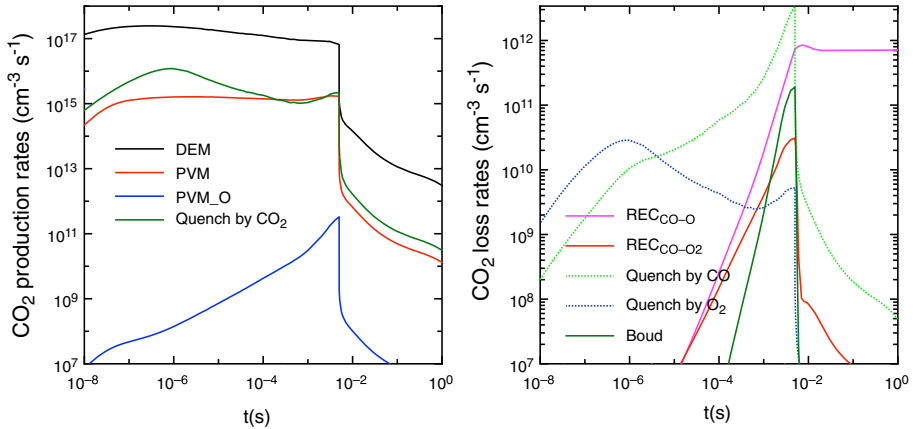


**Fig. 14** CO<sub>2</sub> production and loss rates (cm<sup>-3</sup> s<sup>-1</sup>) in glow discharge conditions ( $P=5$  torr,  $T_{\text{gas}}^{\text{exp}}(t)$ ,  $P_d=1$  Wcm<sup>-3</sup>,  $t_d=5$  ms)

## Contribution of the CO( $a^3\Pi$ ) to CO<sub>2</sub> Dissociation

The new reactive quenching processes introduced for the CO( $a^3\Pi$ ) state give also a contribution to production and loss of CO<sub>2</sub> molecules. In particular,

1. The quenching of the CO( $a^3\Pi$ ) state by collisions with CO<sub>2</sub> in the ground state, i.e.  $\text{CO}(a^3\Pi) + \text{CO}_2 \rightarrow 2\text{CO} + \text{O}$  can be seen as another dissociation mechanism for CO<sub>2</sub>, i.e. dissociation induced by the excitation of the CO( $a^3\Pi$ ) state.
2. The quenching processes of CO( $a^3\Pi$ ) by collisions with O<sub>2</sub> and CO, i.e.  $\text{CO}(a^3\Pi) + \text{O}_2 \rightarrow \text{CO}_2 + \text{O}$  and  $\text{CO}(a^3\Pi) + \text{CO} \rightarrow \text{CO}_2 + \text{C}$  can be considered as back-reactions which reform CO<sub>2</sub>.

Their correspondent rates can be compared to the other CO<sub>2</sub> loss and production rates in order to understand their relative importance. The list of all the production and loss processes for the CO<sub>2</sub> density accounted in the model is presented in Table 5. Figure 13 shows the time evolution of the corresponding rates in the MW test case. In the early time range of the discharge, the quenching by CO<sub>2</sub> prevails up to 10<sup>-5</sup> s due to the initially high CO( $a^3\Pi$ ) concentration, followed by DEM one up to 2–3 10<sup>-4</sup> s. After that, PVM mechanisms overcome the other ones showing the importance of vibrational excitation induced processes in the ms time range. In particular, a prevalence of the PVM<sub>O</sub> process on the PVM one occurs due to the higher PVM<sub>O</sub> rate coefficient and to the increase of O concentration with the CO<sub>2</sub> dissociation progress.

In the MW test case, the most important recombination process for CO<sub>2</sub> in the ms time range is  $\text{CO} + \text{O}_2 \rightarrow \text{CO}_2 + \text{O}$ , while the two ones involving the CO( $a^3\Pi$ ) state, i.e.  $\text{CO}(a^3\Pi) + \text{CO} \rightarrow \text{CO}_2 + \text{C}$  and  $\text{CO}(a^3\Pi) + \text{O}_2 \rightarrow \text{CO}_2 + \text{O}$ , are one and two orders of magnitude lower, respectively.

Figure 14, instead, shows CO<sub>2</sub> production and loss rates in glow discharge conditions ( $P=5$  torr,  $T_{\text{gas}}^{\text{exp}}(t)$ ,  $t_d=5$  ms,  $P_d=1$  Wcm<sup>-3</sup>). As it can be seen, in these conditions, CO<sub>2</sub> is dissociated essentially by electron impact (DEM) and vibrational induced dissociation



(PVM) and the dissociation by quenching of the  $CO(a^3\Pi)$  with collisions with  $CO_2$  have a minor importance. Note also that  $PVM_O$  mechanism is orders of magnitude lower than previous mechanisms. The  $CO_2$  is instead reformed essentially by means of the quenching process involving the  $CO(a^3\Pi)$  by collisions with CO during the discharge and in the post-discharge by recombination of CO and O atoms.

## Conclusions and Perspectives

In this paper, an in-depth study of the role of  $CO_2$  and CO electronic excited states in the kinetics of  $CO_2$  cold non-equilibrium plasmas was carried out by means of a 0D kinetic model in which the electron Boltzmann equation was solved simultaneously and self-consistently with the state-to-state master equations describing the vibrational states, the electronic excited states and the plasma composition. Besides the 7 and 10.5 eV electronic excitation cross sections of the Phelps database, other  $CO_2$  electronic excited levels have been identified by experiments and theoretical methods. Recently, new added data from the Biagi's Magboltz code to the LXCat database have provided a set of several electronic excitation cross sections for  $CO_2$  in the energy range from 6.5 eV up to 25 eV. A new dissociation model has been proposed based on the use of the Biagi electronic excitation cross sections as fully dissociative ones and the corresponding simulation results have been compared to the results obtained with the dissociation model connected to the Phelps database in typical glow discharge and MW discharge conditions. In glow discharge conditions, where dissociation occurs essentially by electron impact and low vibrational excitation is present, the results of the two models are comparable due to compatibility of the two cross section databases obtained by swarm analysis procedures. In the MW discharge case, instead, some discrepancies start appearing when vibrational excitation becomes important, showing the need to integrate a model based only on dissociation from electronic excited states with a model that takes into account also electron impact dissociation from vibrational excited states. The inclusion in the kinetics of some  $CO_2$  electronic excited states as separate species without considering them as dissociative ones needs the implementation of corresponding kinetic equations. Unfortunately, the lack of data present in literature concerning quenching and radiative processes of these states prevent at the moment the construction of corresponding accurate kinetic description and further experimentally and/or theoretically investigations on these aspects is still necessary.

Due to its important role in the kinetics, a new more accurate kinetic description of the  $CO(a^3\Pi)$  state is presented and tested in MW discharge conditions. The newly added processes affect mostly the kinetics by increasing the  $CO(a^3\Pi)$  in the early time of the discharge (up to  $10^{-4}$  s) through dissociative excitation and dissociative recombination processes. In the ms time range the  $CO(a^3\Pi)$  kinetic is dominated by quenching processes with O, CO,  $CO_2$  and  $O_2$ . The results have shown that a change in the time evolution of the  $CO(a^3\Pi)$  density has a direct effect on the eedf, the electron temperature and the electron impact dissociation rates thanks to the effect of superelastic electronic collisions. A direct effect is also present for the CO vdf, CO vibrational temperature and CO vibrational-induced dissociation rates due to the quenching and VE processes involving the  $CO(a^3\Pi)$  and the CO ground state. The  $CO_2$  vdf and consequently the  $CO_2$  vibrational-induced dissociation rates are only indirectly affected by the change of  $CO(a^3\Pi)$  due to the change in the eedf due to eV processes.

Finally, the contribution of the  $\text{CO}(a^3\Pi)$  state to  $\text{CO}_2$  dissociation is examined in terms of production and recombination (or back-reaction) processes both in MW and glow discharge conditions.

Future investigation on electronic excited states will be performed in conditions in which dissociation of  $\text{CO}_2$  via electronic degrees of freedom is assumed to become the dominant mechanism, i.e. at values of the reduced electric field  $E/N$  of hundreds of Td as reported in [37]. Such conditions are obtained in DBD experiments or, for example, in those experimentally and numerically analyzed by Pokrovskiy et al. [84], in nanosecond capillary discharges ignited in pure carbon dioxide at moderate (10–20 mbar) pressures. The latter ones are characterized by high reduced electric field, high specific deposited energy and high value of dissociation degree and present the so-called phenomenon of fast gas heating (FGH) [113, 114], i.e. the high increase of the gas temperature at sub-microsecond timescale due to the high excitation of the electronic excited states during the discharge and their subsequent quenching towards the translational degrees of freedom. For the future, we should take into account the solution of the gas heating equation for the description also of high pressure and high temperature plasmas. Moreover, an improvement of the  $\text{CO}_2$  vibrational kinetics following the approach of Armenise and Kustova [115, 116] which considers the coupling of the three  $\text{CO}_2$  vibrational modes with the use of possible newly calculated state-to-state vibrational energy transfer rate coefficients [117–119] is desirable.

Future developments will be aimed at introducing in the model the kinetics of negative ions, such as  $\text{O}^-$ , as well as  $\text{CO}^-$  and  $\text{CO}_2^-$ . In particular, the  $\text{O}^-$  production should be taken into account through the dissociative electron attachment processes involving  $\text{CO}_2$  and  $\text{CO}$  molecules, i.e.  $e + \text{CO}_2(X, v) \rightarrow \text{CO} + \text{O}^-$  and  $e + \text{CO}(X^1\Sigma^+, v) \rightarrow \text{CO}^- \rightarrow \text{C}(^3P) + \text{O}-(^2P)$ . Unfortunately, the corresponding cross section of the former is only available for  $v=0$  [22], while for the latter, only the  $v$  dependence of one resonant channel of the intermediate  $\text{CO}^-(X^2\Pi)$  state is available, while the important contribution due the  $\text{CO}^-(A^2\Sigma)$  channel is still lacking, see [38, 120]. However, as recently stated in [121], the dissociative electron attachment involving  $\text{CO}_2$  constitutes one of the main electron loss channel under glow discharge conditions, and, as suggested in [98], the mechanisms involving  $\text{O}^-$ , e.g.  $\text{O}^- + \text{CO}(X^1\Sigma^+) \rightarrow e + \text{CO}_2(^1\Sigma_g^+)$  could have an important contribution to the production of  $\text{CO}_2$  from  $\text{CO}$ . For these reasons, one of the future improvement of the model will be the inclusion in the kinetics of previous processes and of  $\text{O}^-$  formation.

Future developments will be also addressed to the inclusion of surface recombination mechanisms. Actually, the surface recombination of the oxygen atoms at the wall, i.e.  $\text{O} + \text{wall} \rightarrow \frac{1}{2} \text{O}_2$  could be an important loss mechanism for the  $\text{O}$  atoms in the plasma volume, influencing the  $\text{CO}_2$  vibrational distribution as well as the whole kinetics. Such recombination is strongly dependent on the values used for the recombination probability  $\gamma_0$ , which, in turn, depends on the experimental conditions such as wall temperature, gas pressure, discharge current etc. Unfortunately, no fundamental and theoretical studies already exist in literature to provide a self-consistently calculation of the  $\text{O}$  recombination probability by coupling both the surface and volume kinetics, relying on the experimental input for this quantity, often not available, and, in general, the need of benchmark experiments to provide validation test of the surface recombination model used.

The introduction in the kinetics of  $\text{He}$  atoms and their processes not only for explaining the results of Ref. [15] but also to reproduce the behavior of new mixture types of the kind  $\text{CO}_2\text{-N}_2\text{-He-CO}$  [122] could also be interesting.

Finally, we would like to point out that the Boltzmann equation we are using in the kinetic model is the two-term expansion equation developed by Rockwood in the time dependent form. However, the two-term approximation is not applicable in absence of rotational symmetry in the velocity space and when inelastic processes give a significant contribution to electron energy losses, enhancing the anisotropy of the electron distribution. For this reason, the two-term approach is often extended to higher orders, giving rise to multi-term Boltzmann solvers that are typically applied to accurate calculations of electron transport coefficients, also in the framework of swarm analysis experiments [123]. In particular, for the N<sub>2</sub> system, the use of four-term expansion at E/N=70 Td gives differences with the two-term solution of approximately 1, 5 and 30% for the drift velocity, the transverse diffusion coefficient and the electronic rate coefficients, respectively, values being confirmed by the Monte-Carlo approach, see [124]. On the other hand, calculations of the eedf in the two terms expansion in laser mixture CO<sub>2</sub>-N<sub>2</sub>-He-CO give small differences within 2% for drift velocity and characteristic energy as compared with the Monte Carlo approach, see [122, 125]. Multi-term solutions of the electron Boltzmann equation applied to the CO<sub>2</sub> case have been developed by Loffhagen [126] and White et al. [127] and, more recently, by Vass et al. [128] with the comparison with experimental transport coefficient values. Moreover, Monte Carlo Flux (MCF) method has been recently applied to CO<sub>2</sub> and its results compared to two-term and multi-term solutions in CO<sub>2</sub> by Vialetto et al. [89], using also the Biagi database of electron impact cross sections. Differences up to 70% for the rate coefficients of inelastic processes from the two-term solution respect to MCF and multi-term ones have been found, showing the importance of benchmarking the two-term Boltzmann equation with the caution that each method should operate with its most appropriate optimized set of cross sections.

## Appendix

See Tables 6, 7, 8, 9, 10 and 11.

**Table 6** Vibrational and electronic excited states included in the model

|                           | CO <sub>2</sub>               |                               | CO                             |             | O <sub>2</sub>                             |       | C                                      |       | O                           |       |
|---------------------------|-------------------------------|-------------------------------|--------------------------------|-------------|--|-------|--|-------|-----------------------------|-------|
| Vibrational levels        | CO <sub>2</sub> (00v), v ≤ 21 |                               | CO(v), v ≤ 80                  |             | O <sub>2</sub> (v), v ≤ 34                 |       |  |       |                             |       |
|                           | v <sub>b1</sub> (010)         |                               | v <sub>FL1</sub> (020) + (100) |             | v <sub>FL2</sub> (030) + (110)             |       | v <sub>FL3</sub> (040) + (120) + (200) |       |                             |       |
|                           | CO <sub>2</sub>               | CO                            | O <sub>2</sub>                 | C           | O  |       |  |       |                             |       |
|                           | Energy (eV)                   | Energy (eV)                   | Energy (eV)                    | Energy (eV) | Energy (eV)                                |       |  |       |                             |       |
| Electronic excited states | CO <sub>2</sub> (10.5)        | 10.5                          | a <sup>3</sup> Π               | 6.0         | Δ <sub>g</sub>                             | 0.976 | <sup>3</sup> P                         | 0     | <sup>3</sup> P              | 0     |
|                           |                               |                               | d <sup>1</sup> Σ <sup>+</sup>  | 6.863       | b <sup>1</sup> Σ <sub>g</sub> <sup>+</sup> | 1.627 | <sup>1</sup> D                         | 1.263 | <sup>1</sup> D              | 1.976 |
|                           |                               |                               | A <sup>1</sup> Π               | 8.03        |  |       | <sup>1</sup> S                         | 2.684 | <sup>1</sup> S              | 4.19  |
|                           |                               |                               | b <sup>3</sup> Σ <sup>+</sup>  | 10.4        |  |       | <sup>5</sup> S                         | 4.182 | <sup>3</sup> S <sup>0</sup> | 9.146 |
|                           |                               |                               | B <sup>1</sup> Σ <sup>+</sup>  | 10.78       |  |       |  |       | <sup>5</sup> S <sup>0</sup> | 9.521 |
|                           |                               |                               | C <sup>1</sup> Σ <sup>+</sup>  | 11.40       |  |       |  |       |                             |       |
|                           |                               | E <sup>1</sup> Σ <sup>+</sup> | 11.52                          |             |  |       |  |       |                             |       |

**Table 7** Electron impact cross sections for the electron Boltzmann equation

|       |  | References   |
|-------|--|--------------|
|       | <b>CO<sub>2</sub></b>  |              |
| (X1)  | $e + CO_2 \leftrightarrow e + CO_2$  | [20]         |
| (X2)  | $e + CO_2(000) \leftrightarrow e + CO_2(x), x = v_{b1}, v_{FL-j}$  | [82, 83]     |
| (X3)  | $e + CO_2(00v) \leftrightarrow e + CO_2(00\omega)$   | [82, 83](*)  |
| (X4)  | $e + CO_2(000) \leftrightarrow e + CO_2(10.5eV)$   | [82, 83]     |
| (X5)  | $e + CO_2(00v) \leftrightarrow e + e + CO_2^+$   | [82, 83](**) |
| (X6)  | $e + CO_2(00v) \leftrightarrow e + C + O$  | [82, 83](**) |
| (X7)  | $e + CO_2 \rightarrow e + CO(a^3\Pi) + O$  | [107]        |
|       | <b>CO</b>  |              |
| (X7)  | $e + CO \leftrightarrow e + CO$  | [100]        |
| (X8)  | $e + CO(v) \rightarrow CO^-(^2\Pi) \rightarrow e + CO(w)$  | [39]         |
| (X9)  | $e + CO(v) \rightarrow CO^-(^2\Pi) \rightarrow e + C(^3P) + O(^3P)$  | [38]         |
| (X10) | $e + CO(v) \leftrightarrow e + e + CO^+$   | [100](**)    |
| (X11) | $e + CO(0) \leftrightarrow e + CO(X),$<br>$X = a^3\Pi, a'^3\Sigma^+, A^1\Pi, b^3\Sigma^+, B^1\Sigma^+, C^1\Sigma^+, E^1\Sigma^+$ | [100]        |
| (X12) | $e + CO(v) \leftrightarrow e + C + O$  | [129](**)    |
|       | <b>O<sub>2</sub></b>   |              |
| (X13) | $e + O_2 \leftrightarrow e + O_2$  | [130]        |
| (X14) | $e + O_2(v) \rightarrow O_2^-(^2\Pi_g, ^2\Pi_u, ^4\Sigma_u^-, ^2\Sigma_u^-) \rightarrow e + O_2(w)$                              | [41]         |
| (X15) | $e + O_2(v) \rightarrow O_2^* \rightarrow e + 2O(^3P)$   | [40]         |
| (X16) | $e + O_2(v) \rightarrow e + O_2^*(A^3\Sigma_u^+) \rightarrow O(^3P) + O(^3P) + e$  | [131]        |
| (X17) | $e + O_2(v) \rightarrow e + O_2^*(B^3\Sigma_u^-) \rightarrow O(^3P) + O(^1D) + e$  | [132]        |
| (X18) | $e + O_2(v) \rightarrow e + O_2^*(B^3\Sigma_u^-) \rightarrow O(^3P) + O(^3P) + e$  | [132]        |
| (X19) | $e + O_2(v) \rightarrow 2e + O_2^+$  | [133]        |
| (X20) | $e + O_2(v=0) \rightarrow e + O_2(a^1\Delta_g)$  | [130]        |
| (X21) | $e + O_2(v=0) \rightarrow e + O_2(b^1\Sigma_g^+)$  | [130]        |
| (X22) | $e + O_2(v=0) \rightarrow e + O_2(b^1\Sigma_g^+)$  | [130]        |
|       | <b>C</b>   |              |
| (X23) | $e + C \leftrightarrow e + C$  | [134]        |
| (X24) | $e + C(^3P) \leftrightarrow e + C^+$   | [134]        |
| (X25) | $e + C(^3P) \leftrightarrow e + C(X), X = ^1D, ^1S, ^5S^0$   | [134]        |
|       | <b>O</b>   |              |
| (X26) | $e + O \leftrightarrow e + O$  | [135]        |
| (X27) | $e + O(^3P) \leftrightarrow e + O^+$   | [135]        |
| (X28) | $e + O(^3P) \leftrightarrow e + O(X), X = ^1D, ^1S, ^5S^0, ^3S^0$  | [135]        |

(\*) Fridman scaling law; (\*\*) Threshold shifting

**Table 8** Heavy-particle chemical processes

|                       |   | References  | $\alpha$ |
|-----------------------|---|-------------|----------|
| <b>CO<sub>2</sub></b> |   |             |          |
| (C1)                  | $CO_2(00v) + M \rightarrow CO + O + M$  | [30, 31](*) | 1        |
| (C2)                  | $CO_2(00v) + O \rightarrow CO + O_2$    | [30, 31](*) | 0.5      |
| (C3)                  | $CO + O + M \rightarrow CO_2(000) + M$  | [30, 31]    |          |
| (C4)                  | $CO(v) + O_2 \rightarrow CO_2 + O$      | [30, 31](*) | 0.5      |
| (C5)                  | $e + CO_2^+ \rightarrow CO + O$         | [30, 31]    |          |
| (C6)                  | $O + CO + CO_2 \rightarrow CO_2 + CO_2$ | [98]        |          |
| (C7)                  | $O + CO + CO \rightarrow CO_2 + CO$     | [98]        |          |
| (C8)                  | $O + CO + O_2 \rightarrow CO_2 + O_2$   | [98]        |          |
| <b>CO</b>             |   |             |          |
| (C6)                  | $CO(v) + M \rightarrow C + O + M$       | [136]       |          |
| (C7)                  | $CO(v) + CO(w) \rightarrow CO_2 + C$    | [137, 138]  |          |
| (C8)                  | $C + O + M \rightarrow CO + M$          | [30, 31]    |          |
| (C9)                  | $CO^+ + e \rightarrow C + O$            | [30, 31]    |          |
| <b>O<sub>2</sub></b>  |   |             |          |
| (C10)                 | $O_2(v) + O \leftrightarrow 2O + O$     | [139]       |          |
| (C11)                 | $O_2(v) + O_2 \leftrightarrow 2O + O_2$ | [140]       |          |

 (\*) Fridman-Macheret  $\alpha$  model [37]

**Table 9** Vibrational kinetic processes

|                          |   | References |
|--------------------------|---|------------|
| <b>CO<sub>2</sub></b>    |   |            |
| (V1)                     | $CO_2(00v) + M \rightarrow CO_2(00w) + M$                         | [30](*)    |
| (V2)                     | $CO_2(00v) + CO_2(00w) \rightarrow CO_2(00v - 1) + CO_2(00w + 1)$ | [30](*)    |
| (V3)                     | $CO_2(00v) + CO_2(x) \rightarrow CO_2(00v - 1) + CO_2(x')$        | [30](*)    |
| <b>CO<sub>2</sub>-CO</b> |   |            |
| (V4)                     | $CO_2(00v) + CO(w - 1) \rightarrow CO_2(00v - 1) + CO(w)$         | [30](*)    |
| <b>CO</b>                |   |            |
| (V5)                     | $CO(v) + CO(w - k) \rightarrow CO(v - k) + CO(w)$                 | [141–143]  |
| (V6)                     | $CO(v) + CO \rightarrow CO(v - k) + CO$                           | [141–143]  |
| (V7)                     | $CO(v) + C \rightarrow CO(v - 1) + C$                             | [144]      |
| (V8)                     | $CO(v) + O \rightarrow CO(v - 1) + O$                             | [144]      |
| (V9)                     | $CO(v) \rightarrow CO(v - 1) + h\nu$                              | [145]      |
| (V10)                    | $CO(a^3\Pi, w = 0) + CO \rightarrow CO(v = 27) + CO$              | [25]       |
| <b>O<sub>2</sub></b>     |   |            |
| (V11)                    | $O_2(v + 1) + O_2(w) \rightarrow O_2(v) + O_2(w + 1)$             | [146]      |
| (V12)                    | $O_2(v) + O \rightarrow O_2(w) + O$                               | [139]      |
| (V13)                    | $O_2(v) + O_2 \rightarrow O_2(v - 1) + O_2$                       | [146]      |

(\*) SSH scaling law [32]

**Table 10** Electronic excited states optical transitions

|       | <b>CO</b>  | <b>A (s<sup>-1</sup>) [75–78]</b> |
|-------|--|-----------------------------------|
| (E1)  | $CO(a^1\Sigma^+) \rightarrow CO(a^3\Pi) + h\nu$      | $10^4$                            |
| (E2)  | $CO(A^1\Pi) \rightarrow CO(X^1\Sigma^+) + h\nu$      | $10^8$                            |
| (E3)  | $CO(b^3\Sigma^+) \rightarrow CO(a^3\Pi) + h\nu$      | $1.852 \cdot 10^7$                |
| (E4)  | $CO(B^1\Sigma^+) \rightarrow CO(X^1\Sigma^+) + h\nu$ | $1.064 \cdot 10^7$                |
| (E5)  | $CO(B^1\Sigma^+) \rightarrow CO(A^1\Pi) + h\nu$      | $2.0 \cdot 10^7$                  |
| (E6)  | $CO(a^3\Pi) \rightarrow CO(X^1\Sigma^+) + h\nu$      | 133                               |
|       | <b>O</b>   | <b>A (s<sup>-1</sup>) [147]</b>   |
| (E7)  | $O(^3S) \rightarrow O(^3P) + h\nu$                   | $6.116 \cdot 10^8$                |
| (E8)  | $O(^3S) \rightarrow O(^1D) + h\nu$                   | $1.83 \cdot 10^3$                 |
| (E9)  | $O(^3S) \rightarrow O(^1S) + h\nu$                   | 4.61                              |
| (E10) | $O(^5S) \rightarrow O(^1D) + h\nu$                   | $5.32 \cdot 10^{-3}$              |
| (E11) | $O(^5S) \rightarrow O(^3P) + h\nu$                   | $5.56 \cdot 10^3$                 |
| (E12) | $O(^1S) \rightarrow O(^3P) + h\nu$                   | $7.5642 \cdot 10^{-2}$            |
| (E13) | $O(^1S) \rightarrow O(^1D) + h\nu$                   | 1.26                              |
| (E14) | $O(^1D) \rightarrow O(^3P) + h\nu$                   | $7.47535 \cdot 10^{-3}$           |
|       | <b>C</b>   | <b>A (s<sup>-1</sup>) [147]</b>   |
| (E15) | $C(^1S) \rightarrow C(^3P) + h\nu$                   | $2.32 \cdot 10^{-3}$              |
| (E16) | $C(^1S) \rightarrow C(^1D) + h\nu$                   | $5.99 \cdot 10^{-1}$              |
| (E17) | $C(^5S) \rightarrow C(^3P) + h\nu$                   | 29.6                              |

**Table 11** Electronic excited states kinetic processes

|                      |   | References      |
|----------------------|---|-----------------|
| <b>CO</b>            |   |                 |
| (K1)                 | $CO(a^3\Pi) + CO \rightarrow CO(X, v = 27) + CO$                                  | [25]            |
| (K2)                 | $CO(X, v > 27) + CO \rightarrow CO(a^3\Pi) + CO$                                  | [101, 102]      |
| (K3)                 | $e + CO_2^+ \rightarrow CO(a^3\Pi) + O$   | [106, 108, 109] |
| (K4)                 | $CO(a^3\Pi) + O_2 \rightarrow CO + O_2$   | [95, 110, 111]  |
| (K5)                 | $CO(a^3\Pi) + O_2 \rightarrow CO + 2O$  | [95, 110, 111]  |
| (K6)                 | $CO(a^3\Pi) + O_2 \rightarrow CO_2 + O$   | [95, 110, 111]  |
| (K7)                 | $CO(a^3\Pi) + CO_2 \rightarrow CO + CO_2$   | [95, 106]       |
| (K8)                 | $CO(a^3\Pi) + CO_2 \rightarrow 2CO + O$   | [95, 106]       |
| (K9)                 | $CO(a^3\Pi) + O \rightarrow CO + O$   | [112]           |
| (K10)                | $CO(a^3\Pi) + CO \rightarrow CO_2 + C$  | [95, 101, 111]  |
| <b>O</b>             |   |                 |
| (Q2)                 | $O(^1D) + O(^3P) \rightarrow O(^3P) + O(^3P)$                                     | [148]           |
| (Q3)                 | $O(^1S) + O(^3P) \rightarrow O(^1D) + O(^1D)$                                     | [148]           |
| (Q4)                 | $O(^5S) + O(^3P) \rightarrow O(^3P) + O(^3P)$                                     | [149]           |
| <b>C</b>             |   |                 |
| (Q5)                 | $C(^1D) + CO \rightarrow C(^3P) + CO$   | [150]           |
| (Q6)                 | $C(^1S) + CO \rightarrow C(^3P) + CO$   | [150]           |
| (Q7)                 | $C(^5S) + C(^3P) \rightarrow C(^3P) + C(^3P)$                                     | [150]           |
| <b>O<sub>2</sub></b> |   |                 |
| (Q8)                 | $O_2(a^1\Delta_g) + O(0) \leftrightarrow O_2(0) + O(0)$                           | [148]           |
| (Q9)                 | $O_2(a^1\Delta_g) + O_2(0) \leftrightarrow O_2(0) + O_2(0)$                       | [148]           |
| (Q10)                | $O_2(a^1\Delta_g) + O_2(a^1\Delta_g) \leftrightarrow O_2(b^1\Sigma_g^+) + O_2(0)$ | [148]           |
| (Q11)                | $O_2(b^1\Sigma_g^+) + O(0) \leftrightarrow O_2(a^1\Delta_g) + O(0)$               | [148]           |
| (Q12)                | $O_2(b^1\Sigma_g^+) + O_2(0) \leftrightarrow O_2(a^1\Delta_g) + O_2(0)$           | [148]           |
| (Q13)                | $O_2(b^1\Sigma_g^+) + O(0) \leftrightarrow O_2(0) + O(^1D)$                       | [148]           |
| (Q14)                | $O(^1D) + O_2(0) \leftrightarrow O(^3P) + O_2(0)$                                 | [148]           |
| (Q15)                | $O(^1S) + O_2(0) \leftrightarrow O(^3P) + O_2(0)$                                 | [148]           |
| (Q16)                | $O(^1D) + O_2(0) \leftrightarrow O(^3P) + O_2(a^1\Delta_g)$                       | [148]           |

**Acknowledgements** The research leading to these results has received funding from ESA Contract No. 4000139351/22/NL/MG “Development of a state-to-state CFD code for the characterization of the aerothermal environment of Ice Giants planets entry capsules” and from PNRR “Ecosistemi dell’Innovazione per la sostenibilità”, Progetto “Tech4You- Technologies for climate change adaptation and quality of life improvement” codice progetto ECS\_00000009, Spoke 2 – Goal 1 – PP3. The authors are very grateful to Annarita Laricchiuta for the useful discussions on electronic excited states.

**Authors’ contributions** L. D. P. developed the code for CO<sub>2</sub>, performed the numerical simulations, the analysis of the results and the writing of the manuscript. G. C. provided the computational framework. M. C. supervised the work. All the authors contributed to the discussion of the results and reviewed the manuscript.

**Funding** Open access funding provided by Consiglio Nazionale Delle Ricerche (CNR) within the CRUI-CARE Agreement. ESA Contract No. 4000139351/22/NL/MG “Development of a state-to-state CFD code for the characterization of the aerothermal environment of Ice Giants planets entry capsules”. PNRR “Ecosistemi dell’Innovazione per la sostenibilità”, Progetto “Tech4You- Technologies for climate change adaptation and quality of life improvement” codice progetto ECS\_00000009, Spoke 2 – Goal 1 – PP3.

**Availability of data and materials** The data of this study are available from the corresponding author (L. D. P.) upon reasonable request.

## Declarations

**Conflict of interest** The authors declare that they have no conflict of interest.

**Ethical approval** Not applicable.

**Open Access** This article is licensed under a Creative Commons Attribution 4.0 International License, which permits use, sharing, adaptation, distribution and reproduction in any medium or format, as long as you give appropriate credit to the original author(s) and the source, provide a link to the Creative Commons licence, and indicate if changes were made. The images or other third party material in this article are included in the article’s Creative Commons licence, unless indicated otherwise in a credit line to the material. If material is not included in the article’s Creative Commons licence and your intended use is not permitted by statutory regulation or exceeds the permitted use, you will need to obtain permission directly from the copyright holder. To view a copy of this licence, visit <http://creativecommons.org/licenses/by/4.0/>.

## References

- Pietanza LD, Guaitella O, Aquilanti V, Armenise I, Bogaerts A, Capitelli M, Colonna G, Guerra V, Engeln R, Kustova E, Lombardi A, Palazzetti F, Silva T (2021) Advances in non-equilibrium CO<sub>2</sub> plasma kinetics: a theoretical and experimental review. *Eur Phys J D* 75:237
- Spencer LF, Gallimore AD (2011) Efficiency of CO<sub>2</sub> dissociation in a radio-frequency discharge. *Plasma Chem Plasma P* 31:79
- Klarenaar BLM, Engeln R, van den Bekerom DCM, van de Sanden MCM, Morillo-Candas AS, Guaitella O (2017) Time evolution of vibrational temperatures in a CO<sub>2</sub> glow discharge measured with infrared absorption spectroscopy. *Plasma Sources Sci Technol* 26:115008
- Da Silva T, Britun N, Godfroid T, Snyders R (2014) Optical characterization of a microwave pulsed discharge used for dissociation of CO<sub>2</sub>. *Plasma Sources Sci Technol* 23:025009
- den Harder N, van den Bekerom DC, Al RS, Graswinckel MF, Palomares JM, Peeters FJJ, Ponduri S, Minea T, Bongers WA, van de Sanden MCM, van Rooij GJ (2017) Homogeneous CO<sub>2</sub> conversion by microwave plasma: wave propagation and diagnostics. *Plasma Process Polym* 14(6):1600120
- Groen PWC, Wolf AJ, Righart TWH, van de Sanden MCM, Peeters FJJ, Bongers WA (2019) Numerical model for the determination of the reduced electric field in a CO<sub>2</sub> microwave plasma derived by the principle of impedance matching. *Plasma Sources Sci Technol* 28:075016
- Aerts R, Snoeckx R, Bogaerts A (2014) In-situ chemical trapping of oxygen in the splitting of carbon dioxide by plasma. *Plasma Process Polym* 11:985
- Brehmer F, Welzel S, van de Sanden MCM, Engel R (2014) CO and byproduct formation during CO<sub>2</sub> reduction in dielectric barrier discharges. *J Appl Phys* 116:123303
- Ponduri S, Becker MM, Welzel S, van de Sanden MCM, Lofftagen D, Engeln R (2016) Fluid modeling of CO<sub>2</sub> dissociation in a dielectric barrier discharge. *J Appl Phys* 119:093301
- Bak MS, Im S-K, Cappelli M (2015) Nanosecond-pulsed discharge plasma splitting of carbon dioxide. *IEEE Trans Plasma Sci* 43:1002
- Montesano C, Salden TPW, Martini LM, Dilecce G, Tosi P (2023) CO<sub>2</sub> reduction by nanosecond-plasma discharges: revealing the dissociation’s time scale and the importance of pulse sequence. *J Phys Chem C* 127(21):10045–10050
- Nunnally T, Gutsol K, Rabinovich A, Fridman A, Gutsol A, Kemoun A (2011) Dissociation of CO<sub>2</sub> in a low current gliding arc plasmatron. *J Phys D Appl Phys* 44:274009



13. Marieu V, Reynier Ph, Maraffa L, Vennemann D, De Filippis F, Caristia S (2007) Evaluation of SCI-ROCCO plasma wind-tunnel capabilities for entry simulations in CO<sub>2</sub> atmospheres. *Acta Astronaut* 61:604
14. Guerra V, Silva T, Pinhao N, Guitella O, Guerra-Garcia C, Peeters FJJ, Tsampas MN, van de Sanden MCM (2022) Plasmas for in situ resource utilization on Mars: fuels, life support, and agriculture. *J Appl Phys* 132:070902
15. Douat C, Bocanegra PE, Dozias S, Robert E, Motterlini R (2021) Production of carbon monoxide from a He/CO<sub>2</sub> plasma jet as a new strategy for therapeutic applications. *Plasma Process Polym* 18:2100069
16. Capitelli M, Celiberto R, Colonna G, Esposito F, Gorse C, Hassouni K, Laricchiuta A, Longo S (2015) Fundamental aspects of plasma chemical physics: kinetics. Springer series on atomic, optical and plasma physics, vol 85. Springer, New York
17. Capitelli M, Armenise I, Bisceglie E, Bruno D, Celiberto R, Colonna G, D'Ammando G, De Pascale O, Esposito F, Gorse C, Laporta V, Laricchiuta A (2012) Thermodynamics, transport and kinetics of equilibrium and non-equilibrium plasmas: a state-to-state approach. *Plasma Chem Plasma Process* 32:427
18. Pietanza LD, Colonna G, D'Ammando G, Laricchiuta A, Capitelli M (2015) Vibrational excitation and dissociation mechanisms of CO<sub>2</sub> under non-equilibrium discharge and post-discharge conditions. *Plasma Sources Sci Technol* 24:042002 (**Fast Track Communications**)
19. Pietanza LD, Colonna G, Capitelli M (2020) Self-consistent electron energy distribution functions, vibrational distributions, electronic excited states kinetics in reacting microwave CO<sub>2</sub> plasma: an advanced model. *Phys Plasmas* 27(2):23513
20. Itikawa Y (2002) Cross sections for electron collisions with carbon dioxide. *J Phys Chem Ref Data* 31(3):749
21. Deschamps MC, Michaud M, Sanche L (2003) Low-energy electron-energy-loss spectroscopy of electronic transitions in solid carbon dioxide. *J Chem Phys* 119:9628
22. LXCat, LXCat database, <http://lxcat.net>
23. Biagi S (2020) Magboltz-transport of electrons in gas mixtures, [magboltz.web.cern.ch/magboltz/](http://magboltz.web.cern.ch/magboltz/). Accessed 5 October 2020
24. Biagi-v7.1 database, [www.lxcat.net](http://www.lxcat.net). Retrieved 5 October 2020
25. Porshnev PI, Wallart HL, Perrin MY, Martin JP (1996) Modeling of optical pumping experiments in CO: I. time-resolved experiments. *Chem Phys* 213:111–122
26. Rockwood SD (1973) Elastic and inelastic cross-sections for electron-Hg scattering from Hg transport data. *Phys Rev A* 8:2348
27. Elliott CJ, Green AE (1976) Electron energy distributions in e-beam generated Xe and Ar plasmas. *J Appl Phys* 47:2946
28. Colonna G, Capitelli M (2008) Boltzmann and master equations for magnetohydrodynamics in weakly ionized gases. *J Thermophys Heat Transf* 22:414
29. Colonna G, D'Angola A (2022) Two-term Boltzmann equation. In: Chapter 2 in “plasma modeling (second edition) methods and applications. IOP Publishing, UK, series 2053–2563, pp 2-1–2-39
30. Kozak T, Bogaerts A (2014) Splitting of CO<sub>2</sub> by vibrational excitation in non-equilibrium plasmas: a reaction kinetics model. *Plasma Sources Sci Technol* 23:045004
31. Kozak T, Bogaerts A (2015) Evaluation of the energy efficiency of CO<sub>2</sub> conversion in microwave discharges using a reaction kinetics model. *Plasma Sources Sci Technol* 24:015024
32. Schwartz RN, Slawsky ZI, Herzfeld KF (1954) *J Chem Phys* 20:1591
33. Pietanza LD, Colonna G, Capitelli M (2017) Non-equilibrium plasma kinetics of reacting CO: an improved state to state approach. *Plasma Sources Sci Technol* 26:125007
34. Pietanza LD, Colonna G, Capitelli M (2018) Non-equilibrium electron and vibrational distributions under nanosecond repetitively pulsed CO discharges and afterglows: I. optically thick plasmas. *Plasma Sources Sci Technol* 27:095004
35. Pietanza LD, Colonna G, Laricchiuta A, Capitelli M (2018) Non-equilibrium electron and vibrational distributions under nanosecond repetitively pulsed CO discharges and afterglows: II. The role of radiative and quenching processes. *Plasma Sources Sci Technol* 27:095003
36. PHYS4ENTRY Database. <http://phys4entrydb.ba.imip.cnr.it/Phys4EntryDB/>
37. Fridman AA (2008) *Plasma Chemistry*. Cambridge University Press, Cambridge
38. Laporta V, Tennyson J, Celiberto R (2016) Carbon monoxide dissociative attachment and resonant dissociation by electron-impact. *Plasma Sources Sci Technol* 25:01LT04
39. Laporta V, Cassidy CM, Tennyson J, Celiberto R (2012) Electron-impact resonant vibration excitation cross sections and rate coefficients for carbon monoxide. *Plasma Sources Sci Technol* 21:045005

40. Laporta V, Celiberto R, Tennyson J (2015) Dissociative electron attachment and electron-impact resonant dissociation of vibrationally excited O<sub>2</sub> molecules. *Phys Rev A* 91:012701
41. Laporta V, Celiberto R, Tennyson J (2013) Resonant vibrational-excitation cross sections and rate constants for low-energy electron scattering by molecular oxygen. *Plasma Sources Sci Technol* 22:025001
42. Laporta V, Tennyson J, Celiberto R (2016) Calculated low-energy electron-impact vibrational excitation cross sections for CO<sub>2</sub> molecules. *Plasma Sources Sci Technol* 25:06LT02
43. Annusova A, Marinov D, Booth JP, Sirse N, Da Silva ML, Lopez B, Guerra V (2018) Kinetics of highly vibrationally excited O<sub>2</sub>(X) molecules in inductively-coupled oxygen plasmas. *Plasma Sources Sci Technol* 27:045006
44. Pietanza LD, Colonna G, Capitelli M (2020) Extended plateaux in the vibrational and electron distribution functions in discharge and post-discharge in O<sub>2</sub>/O reacting plasmas. *Phys Plasm* 27:093510
45. Pietanza LD, Colonna G, Capitelli M (2020) Kinetics versus thermodynamics on CO<sub>2</sub> dissociation in high temperature microwave discharges. *Plasma Sources Sci Technol* 29(3):35022
46. Pietanza LD, Colonna G, Capitelli M (2022) Non-equilibrium plasma kinetics of CO<sub>2</sub> in glow discharges: a comparison with existing modeling and experimental results. *Plasma Sources Sci Technol* 31:104001
47. Grofulovic M, Silva T, Klarenaar BLM, Morillo-Candas AS, Guitella O, Engeln R, Pintassilgo CD, Guerra V (2018) Kinetic study of CO<sub>2</sub> plasmas under non-equilibrium conditions. II. Input of vibrational energy. *Plasma Sources Sci Technol* 27:115009
48. Silva T, Grofulovic M, Klarenaar BLM, Morillo-Candas AS, Guitella O, Engeln R, Pintassilgo CD, Guerra V (2018) Kinetic study of low-temperature CO<sub>2</sub> plasmas under non-equilibrium conditions. I. Relaxation of vibrational energy. *Plasma Sources Sci Technol* 27:015019
49. Pietanza LD, Colonna G, Capitelli M (2023) Activation of vibrational-induced CO<sub>2</sub> dissociation in cold non-equilibrium plasma. *Plasma Phys Control Fusion* 65:044004
50. Kotov V (2022) Vibrational relaxation and triggering of the non-equilibrium vibrational decomposition of CO<sub>2</sub> in gas discharges. *Plasma Sources Sci Technol* 31:094002
51. Hubin-Franskin M-J, Delwiche J, Leclere B, Roy D (1988) Electronic excitation of carbon dioxide in the 10.5–18 eV range studied by inelastic electron scattering spectroscopy. *J Phys B* 21:3211
52. Green MA, Teubener PJO, Campbell L, Brunger MJ, Hoshino M, Ishikawa T, Kitajima M, Tanaka H, Itikawa Y, Kimura M, Buenker RJ (2002) Absolute differential cross sections for electron impact excitation of the 10.8–11.5 eV energy-loss states of CO<sub>2</sub>. *J Phys B* 35:567
53. Monahan KM, Walker WC (1974) Photoabsorption of solid carbon dioxide from 7 to 12 eV. *J Chem Phys* 61:3886
54. Abe H, Onaka R (1984) Molecular excitons of solid carbon dioxide. *J Phys Soc Jpn* 53:1176
55. Winter NW, Bender CF, Goddard WA III (1973) Theoretical assignments of the low-lying electronic states of carbon dioxide. *Chem Phys Lett* 20:489
56. England WB, Ermler WC (1979) Theoretical studies of atmospheric triatomic molecules. New ab initio results for the <sup>1</sup>Π<sub>g</sub><sup>-1</sup>Δ<sub>g</sub> vertical state ordering in CO<sub>2</sub>. *J Chem Phys* 70:1711
57. Spielfiedel A, Feautrier N, Cossart-Magos C, Chambaud G, Rosmus P, Werner H-J, Botschwina P (1999) Bent valence excited states of CO<sub>2</sub>. *J Chem Phys* 97:8382
58. Spielfiedel A, Feautrier N, Chambaud G, Rosmus P, Werner H-J (1993) The first dipole-allowed electronic transition X<sup>1</sup>Σ<sub>g</sub><sup>+</sup>–X<sup>1</sup>Σ<sub>g</sub><sup>+</sup> of CO<sub>2</sub>. *Chem Phys Lett* 216:162
59. Buenker RJ, Honigmann M, Liebermann H-P, Kimura M (2000) Theoretical study of the electronic structure of carbon dioxide: Bending potential curves and generalized oscillator strengths. *Chem Phys* 113:1046
60. Nakatsuji H (1983) Cluster expansion of the wavefunction. Valence and Rydberg excitations, ionizations, and inner-valence ionizations of CO<sub>2</sub> and N<sub>2</sub>O studied by the SAC and SAC CI theories. *Chem Phys* 75:425–441
61. Lee C-H, Winstead C, McKoy V (1999) Collisions of low-energy electrons with CO<sub>2</sub>. *J Chem Phys* 111:5056
62. Mulligan JF (1951) The lower excited states of carbon dioxide. *J Chem Phys* 19:1428
63. Triana JF, Pelaez D, Hochlaf M, Sanz-Vicario JL (2022) Ultrafast CO<sub>2</sub> photodissociation in the energy region of the lowest Rysberg series. *Phys Chem Chem Phys* 24:14072
64. McDiarmid R, Doering JP (1984) Electronic excited states of CO<sub>2</sub>: an electron impact investigation. *J Chem Phys* 80:648
65. Cvejanovic S, Jureta J, Cvejanovic D (1985) Threshold spectrum of CO<sub>2</sub>. *J Phys B* 18:2541
66. McGlynn SP, Rabalais JW, McDonald JM, Scherr V (1971) Electronic spectroscopy of isoelectronic molecules. II. Linear triatomic groupings containing sixteen valence electrons. *Chem Rev* 71:73

67. Chan WF, Cooper G, Brion CE (1993) The electronic spectrum of carbon dioxide. Discrete and continuum photoabsorption oscillator strengths (6–203 eV). *Chem Phys* 178:401
68. Mu-Tao L, McKoy V (1983) Cross sections for electron impact excitation of the low-lying electron states of CO<sub>2</sub>. *J Phys B: Atom Mol Phys* 16(4):657
69. Kawahara H, Kato H, Hoshino M, Tanaka H, Campbell L, Brunger MJ (2008) Integral cross sections for electron impact excitation of the <sup>1</sup>Σ<sub>u</sub><sup>+</sup> and <sup>1</sup>Π<sub>u</sub> electronic states in CO<sub>2</sub>. *J Phys B: At Mol Opt Phys* 41:085203
70. Green MA, Teubner PJO, Campbell L, Brunger MJ, Hoshino M, Ishikawa T, Kitajima M, Tanaka H, Itikawa Y, Kimura M, Buenker RJ (2002) Absolute differential cross sections for electron impact excitation of the 10.8–11.5 eV energy-loss states of CO<sub>2</sub>. *J Phys B: At Mol Opt Phys* 35:567
71. Kim Y-K (2007) Scaled Born cross sections for excitation of H<sub>2</sub> by electron impact. *J Chem Phys* 126:064305
72. Berkowitz J (2012) Photoabsorption, photoionization, and photoelectron spectroscopy. Academic Press, London
73. Vialeto L. Modeling of plasmas for CO<sub>2</sub> conversion: electron kinetics, chemistry and transport. PhD thesis, Eindhoven University of Technology
74. Polak LS, Slovetsky DI (1976) Electron impact induced electronic excitation and molecular dissociation. *Int J Radiat Phys Chem* 8:257–282
75. Stankovic VV, Ristic MM, Vojnovic MM, Aoneas MM, Poparic GB (2020) Ionization and electronic state excitation of CO<sub>2</sub> in radio-frequency electric field. *Plasma Chem Plasma Process* 40:1621
76. Vojnovic MM, Ristic MM, Stankovic VV, Poparic GB (2019) Electron-induced vibrational excitation of CO<sub>2</sub> in dc electric and magnetic fields. *Phys Rev E* 99:063211
77. Annaloro J, Bultel A (2019) Vibrational and electronic collisional-radiative model in CO<sub>2</sub>-N<sub>2</sub>-Ar mixtures for Mars entry problems. *Phys Plasmas* 26:103505
78. Annaloro J, Bultel A (2014) Vibrational and electronic collisional-radiative model in air for Earth entry problems. *Phys Plasmas* 21:123512
79. Grofulovic M, Alves LL, Guerra V (2016) Electron-neutral scattering cross sections for CO<sub>2</sub>. *J Phys D: Appl Phys* 49:395207
80. Morillo-Candas AS, Silva T, Klarenaar BLM, Grofulovic M, Guerra V, Guaitella O (2020) Electron impact dissociation of CO<sub>2</sub>. *Plasma Sources Sci Technol* 29:01LT01
81. Bogaerts A, Wang W, Berthelot A, Guerra V (2016) Modeling plasma-based CO<sub>2</sub> conversion: crucial role of the dissociation cross section. *Plasma Sources Sci Technol* 25:055016
82. Lowke JJ, Phelps AV, Irwin BW (1973) Predicted electron transport coefficients and operating characteristics of CO<sub>2</sub>-N<sub>2</sub>-He laser mixtures. *J Appl Phys* 44:4464
83. Phelps database (2020). [www.lxcat.net](http://www.lxcat.net). Retrieved 5 October 2020
84. Pokrovskiy GV, Popov NA, Starikovskaia SM (2022) Fast gas heating and kinetics of electronically excited states in a nanosecond capillary discharge in CO<sub>2</sub>. *Plasma Sources Sci Technol* 31:035010
85. Capitelli M, Colonna G, D'Ammando G, Pietanza LD (2017) Self-consistent time dependent vibrational and free electron kinetics for CO<sub>2</sub> dissociation and ionization in cold plasmas. *Plasma Sources Sci Technol* 26:055009
86. Cosby PC, Helm H. *Report AD-A266 464 WL.TR-93-2004* (Dayton, OH: Wright-Patterson Airforce Base)
87. Babaeva NY, Naidis GV (2021) On the efficiency of CO<sub>2</sub> conversion in corona and dielectric-barrier discharges. *Plasma Sources Sci Technol* 30:03LT03
88. Vargas J, Lopez B, Lino da Silva M (2021) Heavy particle impact vibrational excitation and dissociation processes in CO<sub>2</sub>. *J Phys Chem A* 125:493
89. Vialeto L, Viegas P, Longo S, Diomede P (2020) Benchmarking of Monte Carlo flux simulations of electrons in CO<sub>2</sub>. *Plasma Sources Sci Technol* 29:115006
90. D'Ammando G, Colonna G, Capitelli M, Laricchiuta A (2015) Superelastic collision under low temperature plasma and afterglow conditions: a golden rule to estimate their quantitative effects. *Phys Plasmas* 22:034501
91. Giljames JJ, Hoekstra S, Meek SA, Metsala M, van de Meerakker SY-T, Meijer G, Groenenboom GC (2007) The radiative lifetime of metastable CO (a<sup>3</sup>Π, v). *J Chem Phys* 127:221102
92. Jongma RT, Berden G, Meijer G (1997) State-specific lifetime determination of the a<sup>3</sup>Π state in CO. *J Chem Phys* 107:7034
93. Fromentin C (2023) Reaction mechanism for CO<sub>2</sub>-N<sub>2</sub> low-temperature plasmas: the role played by O<sub>2</sub> and N<sub>2</sub> on the CO<sub>2</sub> vibrational kinetics and dissociation. PhD thesis, Universidade De Lisboa, Instituto Superior Tecnico

94. Fromentin C, Silva T, Dias TC, Morillo-Candas AS, Biondo O, Guaitella O, Guerra V (2023) Study of vibrational kinetics of CO<sub>2</sub> and CO in CO<sub>2</sub>-O<sub>2</sub> plasmas under non-equilibrium conditions. *Plasma Sources Sci Technol* 32:024001
95. Silva AF, Morillo-Candas AS, Tejero-del-Caz A, Alves LL, Guaitella O, Guerra V (2020) A reaction mechanism for vibrationally-cold low-pressure CO<sub>2</sub> plasmas. *Plasma Sources Sci Technol* 29:125020
96. Cenian A, Chernukho A, Borodin V, Sliwinski G (1994) Modeling of plasma-chemical reactions in gas mixtures of CO<sub>2</sub> lasers I. Gas decomposition in pure CO<sub>2</sub> glow discharge. *Contrib Plasma Phys* 34:25
97. Morillo-Candas AS, Guerra V, Guaitella O (2020) Time evolution of the dissociation fraction in rf CO<sub>2</sub> plasmas: impact and nature of back-reaction mechanism. *J Phys Chem C* 124:17459
98. Silva T, Morillo-Candas AS, Guaitella O, Guerra V (2021) Modeling the time evolution of the dissociation fraction in low-pressure CO<sub>2</sub> plasmas. *J CO<sub>2</sub> Util* 53:101719
99. Davies PB, Martin PA (1990) Diode-laser spectroscopy of  $\alpha^3\Pi$  CO. *Mol Phys* 70:89
100. Itikawa Y (2015) Cross sections for electron collisions with carbon monoxide. *J Phys Chem Ref Data* 44:013105
101. Dunn O, Harteck P, Dondes S (1973) Isotopic enrichment of carbon-13 and oxygen-18 in the ultraviolet photolysis of carbon monoxide. *J Phys Chem* 77:878
102. Donovan RJ, Husain D (1967) Vibrational excitation of carbon monoxide following quenching of the  $\alpha^3\Pi$  state. *Trans Faraday Soc* 63:2979
103. Bultel A, Schneider IF, Babou Y (2014) CO and C<sub>2</sub> excited states relaxation in CO<sub>2</sub> plasmas derived from a Collisional-Radiative model. *J Phys Conf Ser* 511:012059
104. da Silva ML (2004) Simulation des propriétés radiatives du plasma entourant un véhicule traversant une atmosphère planétaire à vitesse hypersonique: Application à la planète Mars. Ph.D. thesis, Laboratoire ICARE, Université d'Orléans
105. Babou Y, Rivière P, Perrin M-Y, Soufiani A (2009) Spectroscopic data for the prediction of radiative transfer in CO<sub>2</sub>-N<sub>2</sub> plasmas. *J Quant Spectrosc Radiat Transfer* 110:89
106. Skrzypkowski MP, Gougousi T, Johnsen R, Golde MF (1998) Measurement of the absolute yield of CO $\alpha^3\Pi$  + O products in the dissociative recombination of CO<sub>2</sub><sup>+</sup> ions with electrons. *J Chem Phys* 108:8400
107. Wells WC, Borst WL, Zipf EC (1972) Production of CO( $\alpha^3\Pi$ ) and other metastable fragments by electron impact dissociation of CO<sub>2</sub>. *J Geophys Res* 77:69
108. Gougousi T, Golde MF, Johnsen R (1997) Electron-ion recombination rate coefficient measurements in a flowing afterglow plasma. *Chem Phys Lett* 265:399
109. Geoghegan M, Adams NG, Smith D (1991) Determination of the electron-ion dissociative recombination coefficients for several molecular ions at 300 K. *J Phys B* 24:2589
110. Cenian A, Chernukho A, Borodin V, Sliwinski G (1994) Modeling of plasma-chemical reactions in gas mixture of CO<sub>2</sub> lasers I. Gas decomposition in pure CO<sub>2</sub> glow discharge. *Contrib Plasma Phys* 34:25–37
111. Wysong JJ (2000) Measurement of quenching rates of CO( $\alpha^3\Pi$ ,  $v = 0$ ) using laser pump-and-probe technique. *Chem Phys Lett* 329:42
112. Felder W, Morrow W, Young R (1972) CO( $\alpha^3\Pi$ ): rate coefficients for quenching by O( $^3P$ ). *Chem Phys Lett* 15:100
113. Popov NA (2011) Fast gas heating in a nitrogen-oxygen discharge plasma: I. Kinetic mechanism. *J Phys D: Appl Phys* 44:285201
114. Popov NA (2001) Investigation on the mechanism for rapid heating of nitrogen and air in gas discharges. *Plasma Phys Rep* 27:886
115. Armenise I, Kustova EV (2013) State-to-state models for CO<sub>2</sub> molecules: from the theory to an application to hypersonic boundary layers. *Chem Phys* 415:269
116. Armenise I, Reynier P, Kustova E (2016) Advanced models for vibrational and chemical kinetics applied to Mars entry aerothermodynamics. *J Thermophys Heat Transf* 30:705
117. Lombardi A, Faginas-Lago N, Pacifici L, Grossi G (2015) Energy transfer upon collision of selectively excited CO<sub>2</sub> molecules: State-to-state cross sections and probabilities for modeling of atmospheres and gaseous flows. *J Chem Phys* 143:034307
118. Bartolomei M, Pirani F, Laganà A, Lombardi A (2012) A full dimensional grid empowered simulation of the CO<sub>2</sub> + CO<sub>2</sub> processes. *J Comput Chem* 33:1806
119. Lombardi A, Pirani F, Bartolomei M, Coletti C, Laganà A (2019) Full dimensional potential energy function and calculation of state-specific properties of the CO + N<sub>2</sub> inelastic processes within an open molecular science cloud perspective. *Front Chem* 7:309
120. Pietanza LD, Colonna G, Capitelli M (2019) Dissociative electron attachment from vibrationally excited molecules in nanosecond repetitively pulsed CO discharges and afterglows. *Front Chem* 7:163

121. Biondo O, Fromentin C, Silva T, Guerra V, van Rooij G, Bogaerts A (2022) Insights into the limitations to vibrational excitation of CO<sub>2</sub>: validation of a kinetic model with pulsed glow discharge experiments. *Plasma Sources Sci Technol* 31:074003
122. Capitelli M, Gorse C, Berardini M, Braglia GL (1981) Influence of second-kind collisions on electron energy distributions, transport coefficients and the rate coefficients in the laser mixture CO<sub>2</sub>-N<sub>2</sub>-He-CO. *Lett Nuovo Cimento* 31:231
123. Pitchford LC, O'Neil SV, Rumble JR (1981) Extended Boltzmann analysis of electron swarm experiments. *Phys Rev A* 23:294-304
124. Pitchford LC, Phelps AV (1982) Comparative calculations of electron-swarm properties in N<sub>2</sub> at moderate E/N values. *Phys Rev A* 25:540
125. Braglia GL, Baiocchi A (1978) The diffusion and drift of electrons in gases: II. A Monte-Carlo simulation in argon. *Physica B+C* 95:227
126. Loffhagen D (2016) Multi-term and non-local electron Boltzmann equation. *Plasma Model* 2053-2563:3-1-3-30
127. White RD, Robson R, Ness KF (2001) Visualization of ion and electron velocity distribution functions in electric and magnetic fields. *J Phys D: Appl Phys* 34:2205
128. Vass M, Korolov I, Loffhagen D, Pinhao N, Donko Z (2017) Electron transport parameters in CO<sub>2</sub>: scanning drift tube measurements and kinetic computations. *Plasma Sources Sci Technol* 26:065007
129. Cosby PC (1993) Electron-impact dissociation of carbon monoxide. *J Chem Phys* 98:7804
130. Ionin AA, Napartovich AP, Yuryshv NN (2007) Physics and engineering of singlet delta oxygen production in low-temperature plasma. *J Phys D: Appl Phys* 40:R25-R61
131. Capitelli M, Celiberto R (1998) Electron-molecule cross sections for plasma applications: the role of internal energy of the target. In: Becker KH (ed) *Novel aspects of electron-molecule collisions*, pp 283-323
132. Laricchiuta A, Celiberto R, Capitelli M (2000) Electron impact cross-sections for electronic excitation of vibrationally excited O<sub>2</sub> to B<sup>3</sup>Σ<sub>u</sub><sup>-</sup> state. *Chem Phys Lett* 329:526-532
133. Kosarim AV, Smirnov BM, Capitelli M, Laricchiuta A, Paniccia F (2006) Electron impact ionization cross sections of vibrationally and electronically excited oxygen molecules. *Chem Phys Lett* 422:513-517
134. Wang Y, Zatsarinny O, Bartschat K (2013) B-spline R-matrix-with pseudostates calculations for electron-impact excitation and ionization of carbon. *Phys Rev A* 87:012704
135. Laher RR, Gilmore FR (1990) Updated excitation and ionization cross sections for electron impact on atomic oxygen. *J Phys Chem Ref Data* 19:277
136. Macdonald RL, Munafò A, Johnston CO, Panesi M (2016) Nonequilibrium radiation and dissociation of CO molecules in shock-heated flows. *Phys Rev Fluids* 1:043401
137. Essenigh KA, Utkin YG, Bernard C, Adamovich IV, Rich JW (2006) Gas phase Boudouard disproportionation reaction between highly vibrationally excited CO molecules. *Chem Phys* 330:506-514
138. Barreto PR, Euclides HDO, Albernaz AF, Aquilanti V, Capitelli M, Grossi G, Lombardi A, Macheret S, Palazzetti F (2017) Gas phase Boudouard reactions involving singlet-singlet and singlet-triplet CO vibrationally excited states: implications for the non-equilibrium vibrational kinetics of CO/CO<sub>2</sub> plasmas. *Eur Phys J D* 71:259
139. Esposito F, Armenise I, Capitta G, Capitelli M (2008) O-O<sub>2</sub> state-to-state vibrational relaxation and dissociation rates based on quasiclassical calculations. *Chem Phys* 351:91-98
140. Cacciatore M, Capitelli M, Dilonardo M (1979) Non equilibrium vibrational population and dissociation rates of oxygen in electrical discharges—the role of atoms and of the recombination process. *Beitraege aus der Plasmaphysik* 18(5):279-299
141. Plonjes E, Palm P, Chernukho AP, Adamovich IV, Rich JW (2000) Time-resolved Fourier transform infrared spectroscopy of optically pumped carbon monoxide. *Chem Phys* 256:315-331
142. Adamovich IV, Macheret SO, Rich JW, Treanor CE (1998) Vibrational energy transfer rates using a forced harmonic oscillator model. *J Therm Heat Transf* 12:57-65
143. Cacciatore M, Billing GD (1981) Semiclassical calculation of VV and VT rate coefficients in CO. *Chem Phys* 58:395-407
144. Schmailzl U, Capitelli M (1979) Nonequilibrium dissociation of CO induced by electron-vibration and IR-laser pumping. *Chem Phys* 41:143-151
145. Langhoff SR, Bauschlicher CW Jr (1995) Global dipole moment function for the X<sup>1</sup>Σ<sup>+</sup> ground state of CO. *J Chem Phys* 102:5220-5225
146. Billing GD, Kolesnick RE (1992) Vibrational relaxation of oxygen. State to state rate constant. *Chem Phys Lett* 200:382-386
147. National Institute of Standards and Technology, Atomic Spectra Database (NIST)
148. Capitelli M, Ferreira CM, Gordiets BF, Osipov AI (2000) *Plasma kinetics in atmospheric gases*

149. Diamy AM, Gonzalez-Flesca N, Legrand JC (1986) Formation et desactivation par l'oxygene moleculaire de l'atome metastable  $O(^5S)$  dans une decharge oxygene-helium. *Spectrochim Acta B* 41(4):317–325
150. Donovan RJ, Husain D (1970) Recent advances in the chemistry of electronically excited atoms. *Chem Rev* 70:489–516

**Publisher's Note** Springer Nature remains neutral with regard to jurisdictional claims in published maps and institutional affiliations.